

THE CHEMICAL COMPOSITIONS AND TEXTURES OF
MATRICES AND CHONDRULE RIMS OF
UNEQUILIBRATED ORDINARY
CHONDRITES—II. THEIR CONSTITUENTS AND
THE IMPLICATIONS FOR THE FORMATION
OF MATRIX OLIVINE

Satoshi MATSUNAMI, Hiroshi NISHIMURA and Hideo TAKESHI

*Department of Geosciences, Faculty of Science, Naruto University of Education,
Takashima, Naruto 772*

Abstract: The micron-size constituents of fine-grained matrices and chondrule rims in ten unequilibrated ordinary chondrites, Semarkona (LL3), Krymka (L3), Sharps (H3), Chainpur (LL3), Tieschitz (H3), Mezö-Madaras (L3), ALH-764 (LL3), ALH-77214 (L3), ALH-77216 (L3), Yamato-790448 (LL3), have been investigated in detail. Special emphasis is put on the mode of occurrence and mineral chemistry of micron-sized matrix olivine in six primitive type-3 ordinary chondrites having lower petrologic subtypes (Krymka, Chainpur, Sharps, Tieschitz, ALH-764 and Yamato-790448).

Textural evidences concerning occurrence of matrix ferrous olivine observed in matrices of chondrite samples studied here seem to indicate that some of matrix intermediate to Fe-rich olivine would have formed through solid-solid reactions between matrix enstatite, silica-rich spherules and metallic Fe-Ni. It is shown that the MnO content increases remarkably with increasing FeO content, showing a strong positive correlation of Mn with Fe in matrix ferrous olivine. The ratios of MnO to FeO appear to be distributed around solar ratio and lower than those of chondrule olivines. Although the solid-solid reaction hypothesis explains a wide variation of Fa mole % of matrix olivine, it is not clear whether reactions between matrix enstatite, silica-rich spherules and metallic Fe-Ni can explain the positive correlation of Mn with Fe in matrix ferrous olivine. Direct vapour→solid condensation is suggested as an alternative mechanism for the formation of matrix ferrous olivine.

1. Introduction

The compositional and petrologic studies of fine-grained matrices and chondrule rims in type-3 ordinary chondrites have been conducted by many investigators (ASHWORTH, 1977; ALLEN *et al.*, 1980; HUSS *et al.*, 1981; IKEDA *et al.*, 1981; NAGAHARA, 1984; MATSUNAMI, 1984; SCOTT *et al.*, 1984; HUTCHISON *et al.*, 1987; ALEXANDER *et al.*, 1989a, b; BREARLEY *et al.*, 1989). The diversity of origins for chondrite matrix materials has been demonstrated by these authors (*e.g.*, SCOTT *et al.*, 1988). The most remarkable feature of opaque matrix in type-3 ordinary chondrites is the FeO-rich nature in chemical composition. Intermediate to Fe-rich olivine is the most abundant and ubiquitous mineral in the matrices and rims of primitive type-3 ordina-

ry chondrites (HUSS *et al.*, 1981; NAGAHARA, 1984). It is suggested that it may be the low temperature condensate from the solar nebula proposed by LARIMER and ANDERS (1967, 1970). IKEDA *et al.* (1981) considered that matrix intermediate olivine may be a low temperature condensate obtained by the solid-gas reaction among enstatite, metallic Fe and nebular gas in the cooling nebula.

Recently, it has been revealed that most characteristics of the matrix materials in primitive type-3 chondrites would have been established by condensation processes including various solid-gas and solid-solid reactions. NAGAHARA (1984) made a detailed petrologic study on matrices in type-3 ordinary chondrites and showed that the matrices are records of condensation and reaction processes in the cooling nebula. She discussed that the saturation or enrichment of silica in the nebular gas is necessary to the formation of matrix Fe-rich olivine. KORNACKI and WOOD (1984) examined the mineral chemistry of matrix olivine in the Allende carbonaceous chondrite and concluded that the matrix olivine seems to have formed through direct vapour→solid condensation.

In this study we present a petrographical study on texture, mode of occurrence and chemical compositions of the micron-size constituents of matrices and rims in ten type-3 ordinary chondrites including those of lower petrologic subtypes, having low thermoluminescence (TL) sensitivities (SEARS *et al.*, 1980, 1982; SEARS and WEEKS, 1983). A detailed study on mode of occurrence and mineral chemistry of micron-sized matrix ferrous olivine was carried out. It may give clues to the possible formation processes of matrix materials in unequilibrated ordinary chondrites (UOCs), because matrix olivine is the most predominant phase in them. Importance of the MnO content in matrix ferrous olivine is emphasized to reexamine the existing ideas on the formation of matrix intermediate to Fe-rich olivine and to discuss the diversity of origins for matrix olivine in UOCs.

2. Samples and Analytical Procedure

Table 1 lists sources and sample numbers of ten type-3 ordinary chondrites studied in this work. These samples are six falls and four Antarctic finds. They are fresh or slightly weathered ones. All meteorites studied except ALH-77216 and Mezö-Madaras belong to the less metamorphosed varieties of type-3 ordinary chondrites (SEARS *et al.*, 1980, 1982; SEARS and WEEKS, 1983). ALH-764 and Yamato-790448 are also belonging to the least equilibrated ones (SEARS and WEEKS, 1983; KOJIMA *et al.*, 1985). Like other very primitive UOCs, they contain abundant fine-grained opaque matrix. The seven chondrite samples belonging to the primitive UOCs (Semarkona, Krymka, Sharps, Chainpur, Tieschitz, ALH-764 and Yamato-790448) were selected for measurement of chemical compositions of the micron-size constituents such as minerals (olivine, pyroxenes), Fe, Al-rich materials and silica-rich objects in opaque matrices and rims.

Six polished thin sections except for Tieschitz, Mezö-Madaras, ALH-764 and Y-790448 were newly prepared. After microscopic study, textures of matrix materials in all samples were studied in detail. For the purpose of investigating the textures of matrix materials, scanning electron microscopy (SEM) and X-ray energy dispersive spectroscopy (EDS) were fully utilized to identify individual matrix constituents and

Table 1. List of chondrite samples studied.

Meteorite	Sample No.	Petrologic subtype ¹	Source of chips and polished thin sections
ALH-764		LL3.3	NIPR (pts)
ALH-77214		L3.4 or 3.5	NIPR (chip)
ALH-77216		L3.8	NIPR (chip)
Yamato-790448			NIPR (pts)
Chainpur	USNM 1251	LL3.4	SI ² (chip)
Krymka	USNM 2488	L3.0	SI (chip)
Mezö-Madaras	USNM 4838-3	L3.7	SI (pts)
Semarkona	USNM 1805	LL3.0	SI (chip)
Sharps	BM ³	H3.4	SI (chip)
Tieschitz	USNM 3093-2	H3.6	SI (pts)

¹: petrologic subtype: SEARS *et al.* (1980, 1982), SEARS and WEEKS (1983).

²: Smithsonian Institution.

³: This sample was provided by Dr. B. MASON.

to select positions for analyses of matrix materials. Details of the SEM-EDS analysis have already been described in MATSUNAMI (1984). Point analyses of olivine, pyroxenes and other constituents in chondrules and matrix materials of selected samples were performed on the automated JEOL JXA-733 electron microprobe analyzer of the Ocean Research Institute of the University of Tokyo, using crystal spectrometers. Operating conditions of the WDS analyses (WDA) of silicates and oxides were 15 kV, 12 nA, a focussed beam diameter of about 1 μm and the empirical BENCE-ALBEE (1968) correction procedure. Since the grain size of matrix materials was mostly less than 10 μm , the contamination of nearby materials for analysis of a small grain was carefully checked with the stoichiometry of the mineral to obtain reliable analytical data.

3. Mode of Occurrence, Textures and Chemical Compositions of Matrix Constituents

The fine-grained opaque matrices and rims in primitive UOCs are mineralogically porous aggregates of ferrous olivine, typically Fa_{35-65} in these chondrites, and minor Ca-poor pyroxene, Ca-rich pyroxene, sodic plagioclase-like materials, Fe, Al-rich materials, silica-rich spherules, metallic Fe-Ni, troilite, magnetite, graphite and other accessory minerals (anorthite, whitlockite, spinel and calcite) (HUSS *et al.*, 1981; IKEDA *et al.*, 1981; NAGAHARA, 1984; MATSUNAMI, 1984). Larger grains ($> \sim 2 \mu\text{m}$) in matrices and rims were identified by the SEM-EDS technique. In this paper we define "matrix materials" in UOCs as finer grains than about 20 μm , although larger grains ($> 1 \mu\text{m}$) may be chondrule fragments (ALEXANDER *et al.*, 1989a; BREARLEY *et al.*, 1989). Especially, olivine and Ca-poor pyroxene are the abundant minerals in matrix and chondrule rim that are large (2–20 μm in diameter) enough for accurate analyses by the WDS method. Recently, HUTCHISON *et al.* (1987) have showed that some of the fine-grained FeO-rich silicates in Semarkona are composed of smectite by a transmission electron microscope (TEM).

3.1. Olivine

Olivine is the most abundant and ubiquitous mineral in the matrices and rims of UOCs. Typical occurrences of micron-sized olivine are shown in Figs. 1–6. Representative occurrences concerning their formation processes observed in opaque matrices of chondrite samples studied here are classified into four types: (1) subround to angular single grains with or without compositional zoning, (2) intermediate olivine ($Fa_{\sim 50}$) overgrown on enstatite, (3) intermediate to Fe-rich olivine overgrown on Fe-Ni metal aggregate and (4) Fe-rich olivine overgrown on silica-rich spherule. Figure 1 shows angular to subround micron-sized olivine and pyroxene grains embedded in micron-sized silicate grains in opaque matrix of Krymka. Figure 2 illustrates that intermediate olivine (Fa_{50}) overgrows on an irregular grain of Ca-poor pyroxene ($Wo_1Fs_{14}En_{85}$) in opaque matrix of Chainpur. It appears that Fe ions derived from an aggregate of Fe-Ni metals and troilite would have reacted with the pyroxene grain to produce micron-sized intermediate olivine. Figure 3 provides an interesting example of a texture showing that micron-sized intermediate olivine (Fa_{51-52}) rimming a metallic aggregate composed of kamacite (Ni 4.0 wt%, Co 1.91 wt%) and taenite (Ni 52.4 wt%) in Chainpur matrix. This olivine has magnesian core (Fa_{14}) (dark part of olivine in the figure). Figure 4 shows that intermediate olivine (Fa_{58-59}) overgrows on an aggregate of fine-grained taenite (Ni 45.3 wt%) in matrix of Y-790448. This olivine has submicron-size inclusions enriched in Al and Na. Figure 5 shows that Fe-rich olivine (Fa_{70} , MnO=0.7 wt%) overgrows on a silica-rich material ($SiO_2=93$ wt%, FeO=5 wt%, MnO<0.1 wt%, MgO=1.7 wt%) in opaque matrix of Sharps. Figure 6 shows olivine grains in Y-790448 matrix having thin rinds of ferrous olivine. Figure 1 also presents a remarkable example of asymmetric compositional zoning of relatively large matrix olivine in Krymka, showing that a magnesian (Fa_{10-11}) part (dark) is partially enveloped by a thick part of Fe-rich olivine (Fa_{40-78}) (bright) with gradual compositional change.

Figure 7 shows comparison of Fa mole% between chondrule olivine and micron-sized matrix olivine in four representative samples. For example, Krymka (L3.0) is characterized by the presence of matrix olivine grains of highly variable composition (Fa_{6-96}), compared to magnesian chondrule olivine (Fa_{0-26}). On the other hand, ALH-77216 (L3.8) is distinguished from Krymka by similar compositional range of matrix olivine to that of chondrule olivine, indicating increasing degree of equilibration between chondrule olivine and matrix olivine. In other chondrite samples, the relations of compositional ranges of both chondrule and matrix olivines seem to show intermediate features between the above extreme two.

Histograms of micron-sized matrix olivine composition in six chondrite samples are shown in Fig. 8. HUSS *et al.* (1981) and NAGAHARA (1984) have already reported the compositional variations of matrix olivine in several samples studied here. Olivine grains in matrices of primitive UOCs have a wide compositional range: compositions vary through Fa_{3-96} (Fig. 8), with mean compositions ranging from Fa_{38} to Fa_{50} . Olivine in opaque matrix of Krymka exhibits a remarkably wide range of composition (Fa_{6-96}), which is uniformly distributed in the whole range of composition. Matrix olivine in Sharps and Y-790448 has similar compositional ranges, which are slightly more narrow: Fa_{3-50} for Sharps and Fa_{7-56} for Y-790448, respectively. Olivine in

Fig. 1. SEM photograph of opaque matrix and chondrule rim of Krymka, showing a representative mode of occurrence of matrix olivine and pyroxene. Micron-sized angular grains of olivine and pyroxene are present. A large grain of matrix olivine with an asymmetrical zoning (zoned ol) is also observed.

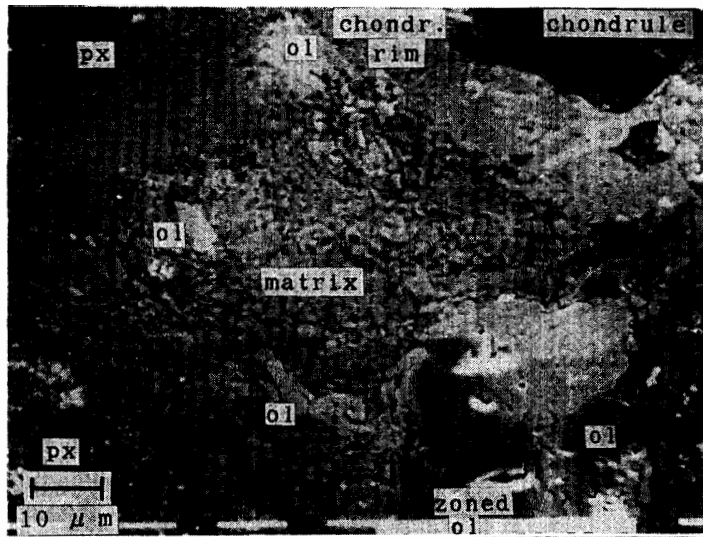


Fig. 2. SEM photograph of intermediate olivine overgrown on an irregular grain of magnesian pyroxene in Chainpur matrix, in contact with a large aggregate of metallic Fe-Ni and troilite, suggesting that the olivine would have formed through the reaction between enstatite and metallic Fe-Ni.

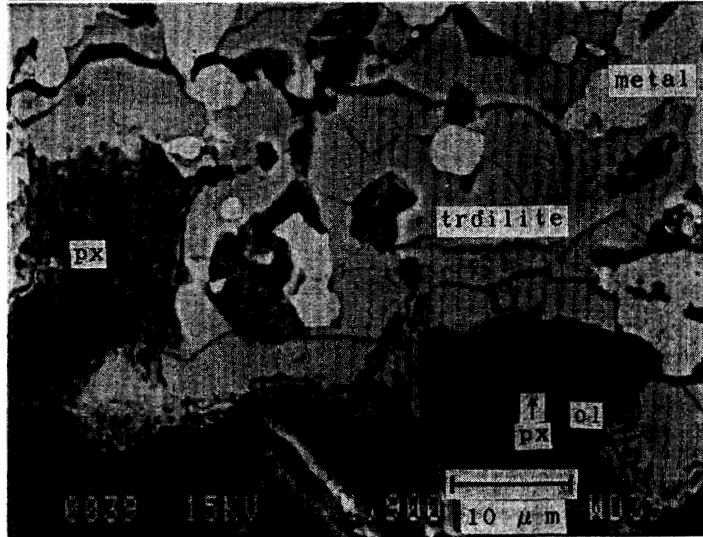
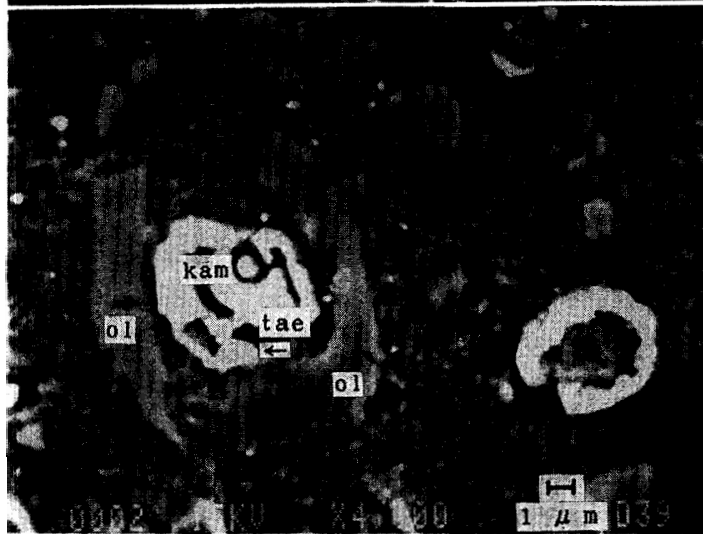


Fig. 3. SEM photograph of intermediate olivine enveloping a micron-sized spherical aggregate of kamacite and taenite in Chainpur matrix.



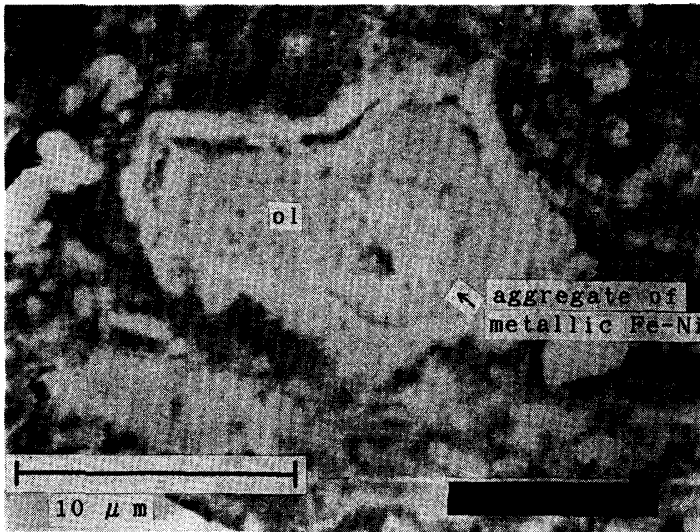


Fig. 4. SEM photograph of intermediate olivine overgrown on a fine-grained aggregate of taenite in matrix of Yamato-790448, including submicron-sized objects enriched in Al and Na (gray spots in olivine).

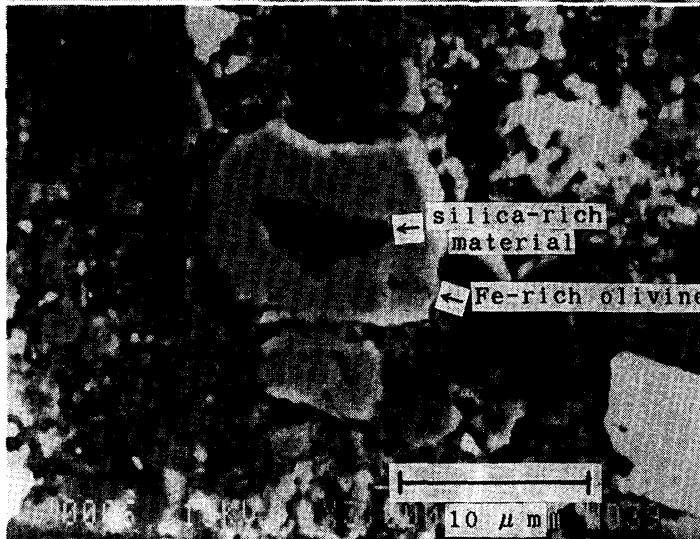


Fig. 5. SEM photograph of Fe-rich olivine overgrown on a micron-sized silica-rich object in Sharps matrix, suggesting that the silica-rich materials are closely related to the formation of matrix Fe-rich olivine.

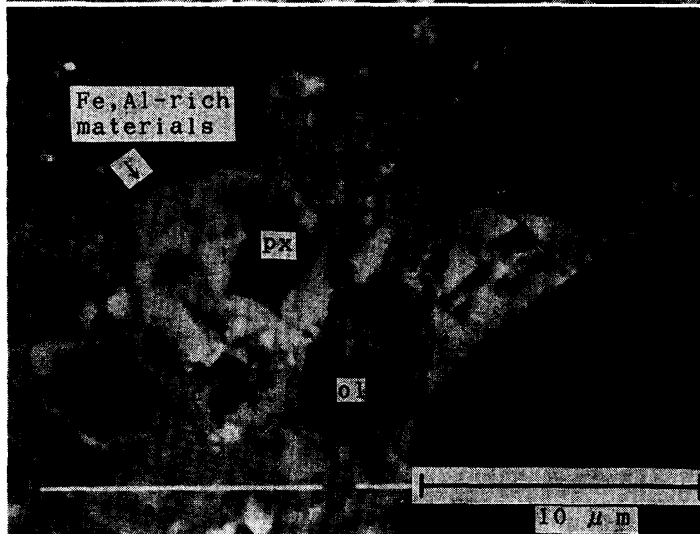


Fig. 6. SEM photograph of micron-sized olivine with compositional zoning in matrix of Yamato-790448. Dark magnesian core is enveloped by a thin rind of ferrous olivine.

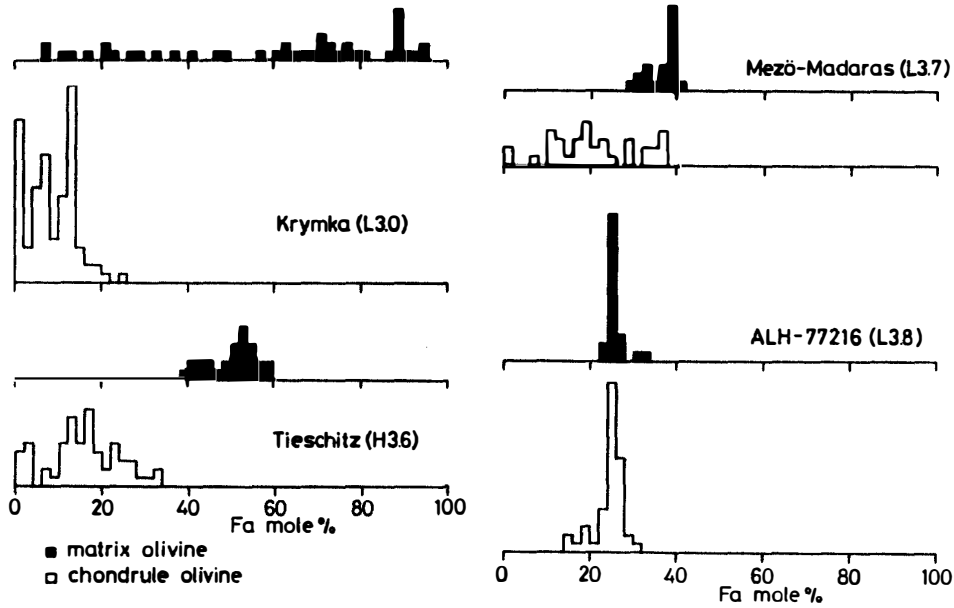


Fig. 7. Comparison of compositional variation of matrix olivine and chondrule olivine in four type-3 ordinary chondrites: Krymka, Tieschitz, Mezö-Madaras and ALH-77216.

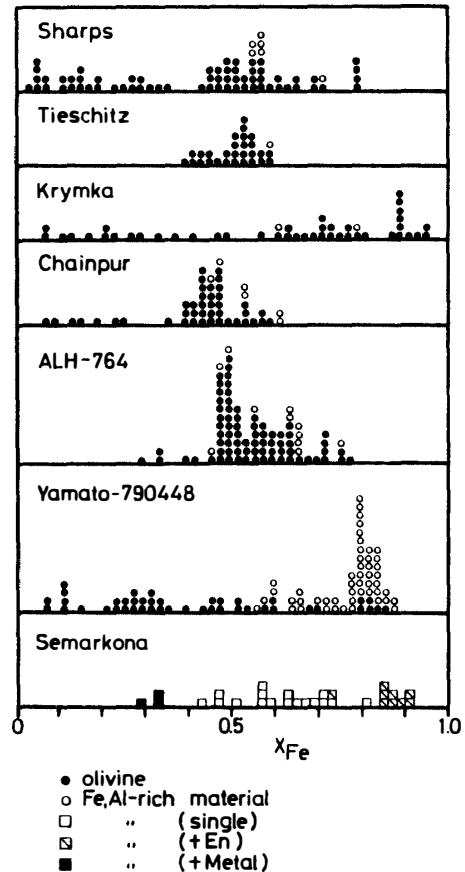


Fig. 8. Frequency diagrams of X_{Fe} [$=Fe^{2+}/(Mg^{2+} + Fe^{2+})$] of analyzed matrix olivine (solid circles) in six type-3 ordinary chondrites: Sharps, Tieschitz, Krymka, Chainpur, ALH-764 and Yamato-790448. Fe, Al-rich materials in matrix (open circles) are also plotted. In addition, Fe, Al-rich materials in Semarkona (squares) are also shown.

Table 2. Representative analyses of matrix olivine in six primitive type-3 ordinary chondrites: Krymka (L3.0), Chainpur (LL3.4), Sharps (H3.4), Tieschitz (H3.6), ALH-764 (LL3.3) and Yamato-790448 (LL3). These data were obtained by the WDA. Apparent diameter of olivine grain (D) is also listed.

Meteorite													
Krymka													
SiO ₂	41.0	40.5	38.6	36.4	35.3	32.9	32.4	32.0	31.2	30.2	29.2	30.3	29.5
Al ₂ O ₃	— ²	.06	—	—	—	.78	.42	.15	.26	.06	.12	.13	.16
Cr ₂ O ₃	—	.16	.06	.10	—	.45	.14	.05	—	.12	.18	.08	—
FeO	7.75	11.6	24.9	31.6	39.6	44.5	50.6	54.0	56.8	62.6	65.2	64.8	65.9
MnO	.81	.28	.23	.36	.30	.38	.45	.51	.53	.62	.65	.62	.73
MgO	50.9	48.2	37.0	30.7	24.3	19.1	14.4	12.3	9.72	4.82	4.06	2.65	1.74
CaO	.17	.05	.12	.18	.21	.35	.16	.15	.12	.10	.11	.09	.14
Na ₂ O	—	—	—	—	—	.09	.09	—	.15	—	—	.09	—
NiO	—	—	.07	.05	.09	.75	.53	.16	.24	.43	.23	.51	.41
Total	100.6	100.9	101.0	99.4	99.8	99.3	99.2	99.3	99.0	99.0	99.8	99.3	98.6
X _{Fe} ¹	.079	.119	.274	.367	.477	.567	.664	.711	.766	.879	.900	.932	.955
D [μ m]	7	5	5	10	6	5	6	3	3	4	4	4	5
Meteorite													
Chainpur													
SiO ₂	40.4	39.9	37.9	36.2	35.5	35.1	34.4	34.3	33.5	33.8			
Al ₂ O ₃	—	—	—	.23	—	—	.14	—	—	—			
Cr ₂ O ₃	—	.11	.10	.22	—	.11	.36	.07	—	—			.10
FeO	9.42	15.1	21.8	32.6	36.1	38.2	39.6	43.1	45.7	46.8			
MnO	—	.23	.33	.39	.52	.48	.56	.57	.52	.61			
MgO	50.0	45.4	38.8	29.9	27.3	25.2	24.6	21.0	18.8	19.0			
CaO	.07	.05	.21	.34	.14	.17	.07	.09	.15	.14			
Na ₂ O	—	—	—	—	—	—	—	—	—	—			
NiO	.06	.32	—	.05	—	—	—	—	.08	—			
Total	100.0	101.1	99.1	99.9	99.6	99.3	99.7	99.1	98.8	100.5			
X _{Fe} ¹	.096	.157	.239	.380	.425	.460	.474	.535	.576	.580			
D [μ m]	3	5	21	3	5	4	3	7	7	3			

Table 2 (continued).

Meteorite	Sharps											Tieschitz					
SiO ₂	41.2	39.3	37.4	36.7	35.2	34.7	33.8	33.1	31.9	31.9	31.2	35.0	35.0	34.8	34.1	33.8	33.6
Al ₂ O ₃	.05	—	—	—	—	—	.31	—	.07	.27	.50	—	—	—	—	—	—
Cr ₂ O ₃	— ²	.11	—	.10	.07	.06	.30	.07	.21	.09	.28	—	.07	—	.07	—	—
FeO	5.75	13.3	23.9	31.2	38.1	40.3	43.8	50.7	53.6	57.5	57.5	36.3	38.4	41.6	43.2	44.7	47.3
MnO	—	1.17	.28	.50	.42	.50	.52	.74	.70	.88	.87	.46	.46	.50	.58	.56	.57
MgO	52.9	44.8	37.5	31.2	25.6	23.5	19.6	14.9	12.6	8.71	8.28	26.8	25.3	22.7	21.4	19.8	18.3
CaO	.17	.28	.13	.21	.15	.10	.71	.09	.08	.15	.87	.05	.11	.06	—	.07	.06
Na ₂ O	—	—	—	—	—	.06	.14	—	—	.29	.46	.14	—	—	—	—	—
NiO	.06	—	.11	—	—	—	.08	—	.07	—	.07	—	—	—	—	—	—
Total	100.1	99.0	99.3	99.9	99.5	99.2	99.3	99.6	99.2	99.8	100.0	98.8	99.3	99.7	99.4	98.9	99.8
X _{Fe} ¹	.057	.143	.263	.359	.455	.491	.557	.657	.705	.788	.796	.432	.460	.507	.532	.559	.592
D [μm]	4	4	5	5	7	7	3	5	4 ³	4	2	8	5	10	4	11	13

Meteorite	ALH-764												
SiO ₂	35.2	35.3	35.3	34.8	34.8	33.9	33.9	33.3	33.0	32.8	32.5	31.4	
Al ₂ O ₃	.17	.15	—	.15	—	—	—	.41	—	.35	.07	—	
Cr ₂ O ₃	—	.09	—	.12	.11	.05	.05	.78	.08	.11	.05	—	
FeO	38.8	39.7	40.7	41.5	42.2	45.8	48.0	48.8	51.4	53.2	53.8	57.5	
MnO	.45	.36	.49	.58	.53	.61	.62	.66	.66	.70	.69	.84	
MgO	25.1	24.1	23.2	22.4	22.2	18.8	17.3	15.9	14.7	12.6	12.7	10.2	
CaO	.08	.28	.09	.09	—	—	.10	—	—	.07	.05	.07	
Na ₂ O	—	.05	—	.06	—	—	—	.10	—	.16	.06	—	
NiO	.13	—	.11	.28	.06	.85	—	—	—	—	.15	—	
Total	99.9	100.0	99.9	100.0	99.9	100.0	100.0	100.0	99.8	100.0	100.1	100.0	
X _{Fe} ¹	.465	.480	.496	.510	.517	.577	.609	.632	.662	.703	.705	.760	
D [μm]	3	4	6	4	4	3	4	5	4	4	5	6	

Formation of Matrix Olivine in UCs

Table 2 (continued).

Meteorite												
Yamato-790448												
SiO ₂	40.8	40.5	39.4	38.4	36.9	36.6	35.7	35.6	34.4	33.6	32.9	31.2
Al ₂ O ₃	.53	—	.05	—	.66	.09	.17	—	.15	.76	.50	.55
Cr ₂ O ₃	.23	—	.07	—	.18	—	.05	.10	—	—	.07	.11
FeO	7.65	11.1	18.7	28.7	35.1	38.3	43.7	45.8	51.7	55.4	57.2	60.4
MnO	—	.68	.27	.33	.38	.35	.55	.57	.84	.88	.76	.82
MgO	49.8	47.6	41.0	32.2	25.3	24.4	19.2	17.7	12.6	8.26	7.49	5.73
CaO	.50	.12	.20	.20	.35	.09	.11	.06	.06	.23	.17	.29
Na ₂ O	.22	—	—	—	.80	.07	—	.06	.09	.32	.26	.11
NiO	.10	—	.17	.07	.27	.07	.56	.10	.06	.41	.55	.71
Total	99.8	100.0	99.9	99.9	99.9	100.0	100.0	100.0	99.9	99.9	99.9	99.9
X _{Fe} ¹	.079	.116	.204	.333	.437	.469	.561	.593	.698	.790	.811	.855
D [μ m]	5	6	6	6	4	5	3	10	4	3	3	5

¹: Fe/(Mg+Fe), ²: not detected, ³: thickness of olivine layer on a silica-rich spherule in Fig. 5.

Table 3. Average composition and grain size of matrix olivine in Krymka, Tieschitz, Sharps, Chainpur, ALH-764 and Yamato-790448 chondrites, obtained by WDA.

Meteorite	Krymka				Tieschitz		Sharps		43	
	46		36		28		65		Fa _{>30}	1σ
N	mean	1σ	Fa _{>30} ¹	1σ	mean	1σ	mean	1σ	Fa _{>30}	1σ
SiO ₂	33.9	3.7	32.3	2.1	34.6	1.0	36.1	2.9	34.3	1.4
Al ₂ O ₃	.17	.19	.20	.20	.08	.15	.08	.12	.09	.15
Cr ₂ O ₃	.13	.21	.15	.23	.11	.20	.10	.11	.11	.13
FeO	45.2	19.3	53.7	11.0	41.6	3.8	33.5	16.2	43.8	7.6
MnO	.47	.18	.50	.14	.52	.08	.48	.25	.59	.15
MgO	19.6	15.9	12.6	9.1	22.9	3.0	29.4	13.6	20.8	6.6
CaO	.14	.07	.14	.07	.10	.11	.19	.16	.20	.19
Na ₂ O	.04	.04	.05	.04	.05	.06	.06	.09	.08	.10
NiO	.30	.24	.35	.24	.07	.19	.05	.04	.05	.04
Total	99.95		99.99		100.03		99.96		100.02	
X _{Fe}	.564	.286	.706	.182	.504	.055	.390	.221	.541	.123
C _{Na-Al} ²			.679		.609				.812	
C _{Fe-Mn} ³			.907		.830				.677	
D [μm]	5.1	2.2	4.8	2.2	7.3	2.8	4.4	1.6	4.3	1.4

Meteorite	Chainpur		ALH-764		Yamato-790448		25			
	42		34		70		40		Fa _{>30}	1σ
N	mean	1σ	Fa _{>30}	1σ	mean	1σ	mean	1σ	Fa _{>30}	1σ
SiO ₂	35.5	2.3	34.8	1.6	34.5	1.4	37.6	2.5	36.3	2.3
Al ₂ O ₃	.15	.19	.17	.20	.17	.21	.14	.22	.18	.26
Cr ₂ O ₃	.17	.15	.19	.16	.16	.16	.08	.07	.08	.07
FeO	34.7	9.9	38.8	4.1	43.9	5.6	31.4	15.2	40.2	11.5
MnO	.47	.11	.49	.06	.56	.11	.45	.22	.54	.20
MgO	28.8	8.1	25.4	3.0	20.5	4.6	30.0	13.2	22.2	10.0
CaO	.10	.07	.11	.07	.11	.12	.15	.10	.15	.09
Na ₂ O	.05	.07	.06	.07	.08	.09	.06	.08	.07	.10
NiO	.03	.04	.04	.04	.09	.14	.18	.20	.25	.23
Total	99.97		100.06		100.07		100.06		99.97	
X _{Fe}	.404	.127	.461	.056	.546	.088	.370	.227	.504	.190
C _{Na-Al} ²			.794		.779				.649	
C _{Fe-Mn} ³			.657		.904				.824	
D [μm]	4.2	1.9	4.1	2.0	5.3	3.0	6.2	2.7	5.8	2.2

¹: average of analyses of matrix Fe-rich olivine (Fa_{>30}).

²: correlation coefficient between Na₂O and Al₂O₃ in ferrous olivine (Fa_{>30}).

³: correlation coefficient between FeO and MnO in ferrous olivine (Fa_{>30}).

Chainpur and ALH-764 also shows wide compositional ranges: compositions vary through Fa₆₋₅₈ for Chainpur and Fa₂₉₋₇₈ for ALH-764, respectively, with broad peaks around Fa₄₀₋₅₀. In contrast, olivine in matrix of Tieschitz chondrite is intermediate and has a narrow range of composition (Fa₄₀₋₅₀).

Representative analyses of micron-sized matrix olivine are listed in Table 2. The average and 1σ of chemical composition and grain size of micron-sized ferrous olivine in opaque matrices of six primitive samples are tabulated in Table 3. For instance, variations of mineal chemistry of matrix olivine are shown for Krymka and Tieschitz

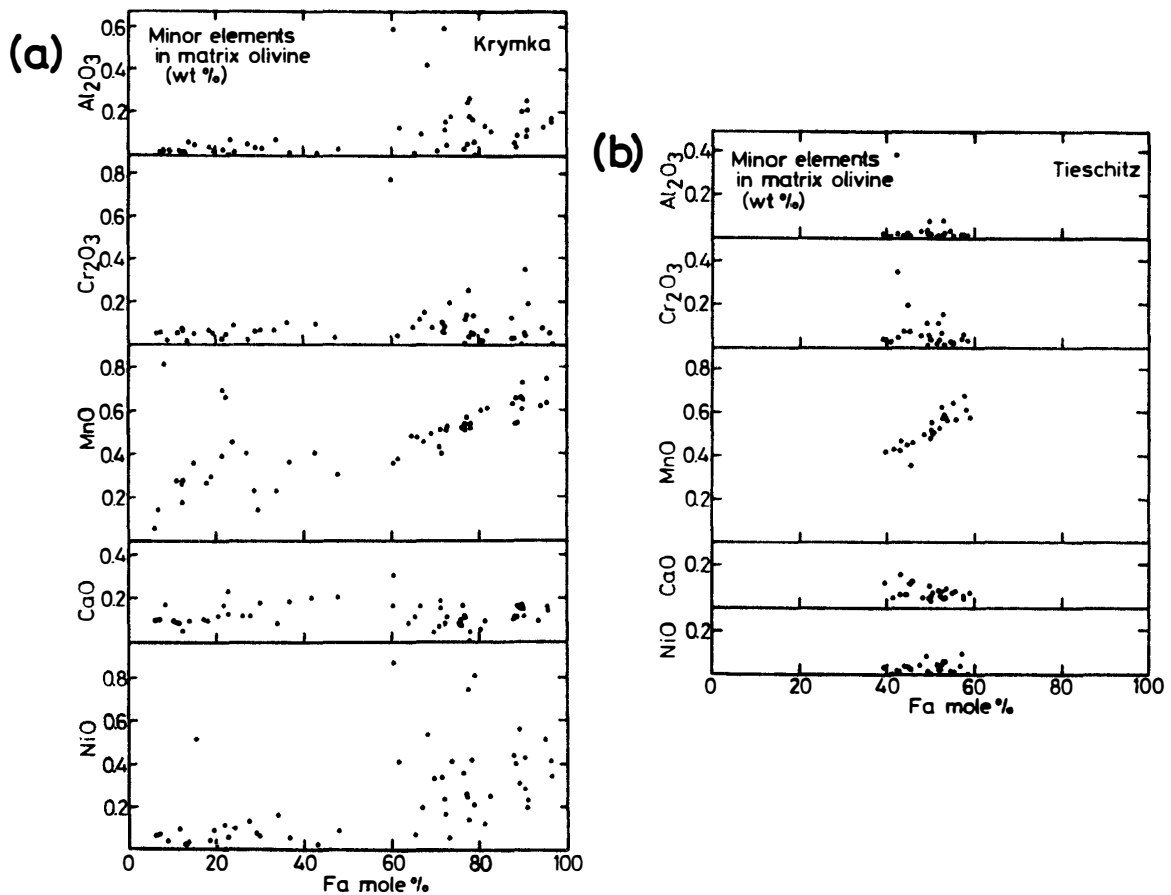


Fig. 9. Variations of minor element contents in matrix olivine of (a) the Krymka and (b) Tieschitz chondrites.

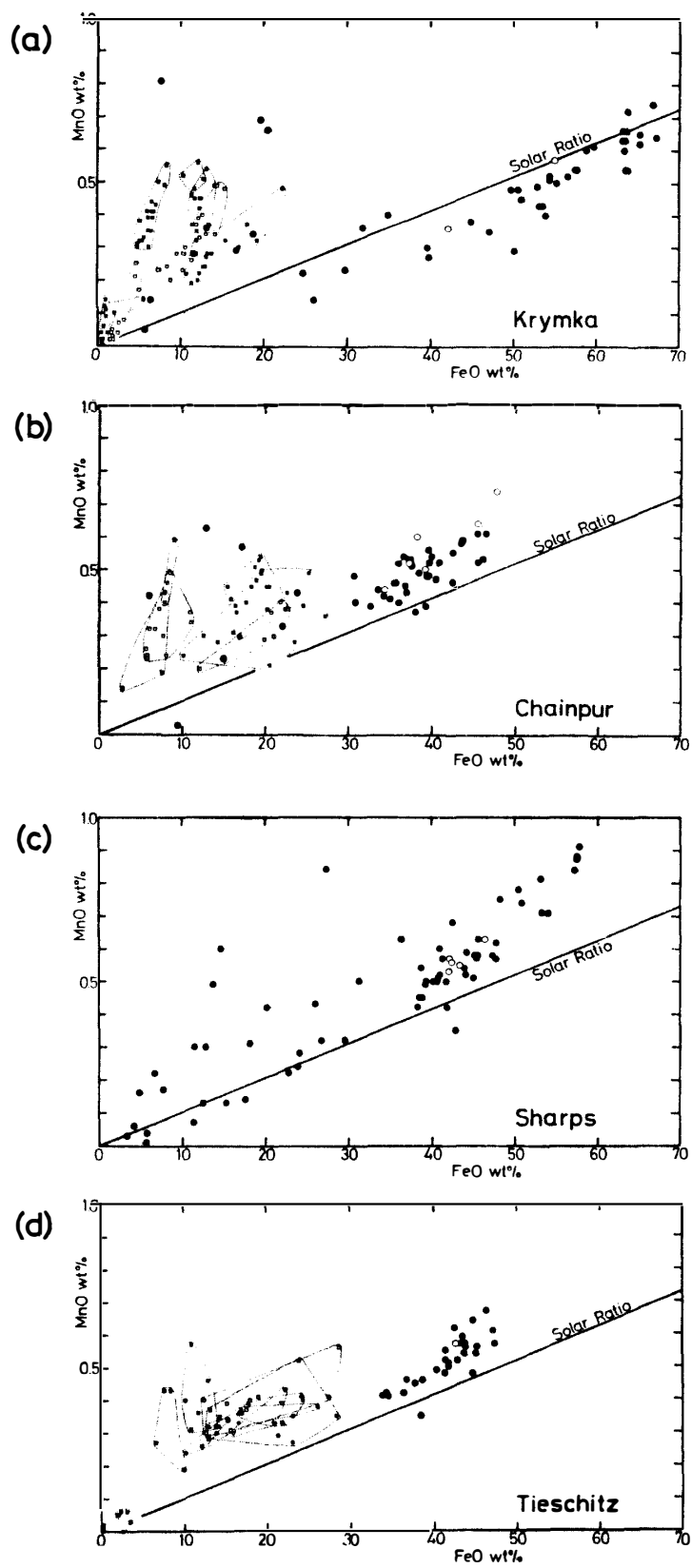
in Fig. 9. Olivine in matrices frequently contains significant amounts of Al_2O_3 (as much as ~ 1.0 wt%) and Na_2O (as much as ~ 0.5 wt%). As shown in Fig. 4, these elements may probably occur in submicron-size inclusions of Al, Na-rich, sodic plagioclase-like material (rather than in the olivine crystal structure). This interpretation is supported by the fact that the Al_2O_3 and Na_2O contents are correlated positively in ferrous olivine ($\text{Fa}_{>30}$); the correlation coefficients range from 0.61 to 0.81 (Table 3). Similarly, the Cr_2O_3 , CaO and NiO contents are sometimes high as much as ~ 1.0 wt%. The high NiO content of some olivine grains may be attributable to small inclusion of Fe-Ni metal or contamination of nearby metallic Fe-Ni grain. Olivine in opaque matrix commonly contains a significant amount of MnO as much as 1.2 wt%. Especially, the MnO content of ferrous olivine ($\text{Fa}_{>30}$) increases remarkably with increasing FeO content. Comparisons of the MnO content of matrix olivine with that of chondrule olivine in several selected chondrules are shown in Fig. 10a-f. As shown in these figures, the positive correlation of MnO with FeO is strikingly clear in ferrous olivine ($\text{Fa}_{>30}$). The correlation coefficients range from 0.66 to 0.91 (Table 3). The ratios of MnO to FeO in ferrous matrix olivines appear to be distributed nearly around solar ratio ($\text{MnO}/\text{FeO} \sim 0.01$; ANDERS and EBIHARA, 1982). On the other hand, chondrule olivines in individual chondrule frequently show a positive correlation of MnO with FeO. The ratio of MnO to FeO in chondrule olivine is, however, generally

Table 4. Representative WDA of matrix olivine with compositional zoning in ALH-764, Yamato-790448 and Krymka chondrites.

Meteorite No.	ALH-764						Yamato-790448					
	pair 1		pair 2		pair 3		pair 4		pair 5			
	core	rim	core	rim	core	rim1	rim2	core	rim	core	rim	
SiO ₂	37.9	35.3	36.0	33.8	34.9	33.2	33.2	38.0	33.8	41.1	36.8	
Al ₂ O ₃	— ²	—	—	.09	—	.16	—	.07	.13	.13	.25	
Cr ₂ O ₃	.05	—	—	.57	.08	.62	.13	.19	.15	—	.05	
FeO	25.8	40.3	29.0	41.6	35.6	46.6	47.4	25.0	50.9	10.9	41.9	
MnO	.31	.55	.26	.54	.25	.56	.62	.51	.64	—	.30	
MgO	35.7	23.7	34.3	23.3	28.7	18.5	18.6	36.0	13.7	47.7	20.3	
CaO	.23	—	.24	.06	.22	.10	—	—	.05	—	.12	
NiO	.08	—	.08	—	.14	.09	.05	.13	.57	.07	.11	
Total	100.1	99.9	99.9	100.0	99.9	99.8	100.0	99.9	99.9	99.9	99.8	
X _{Fe} ¹	.289	.488	.321	.500	.410	.585	.588	.280	.676	.114	.536	

Meteorite No.	Krymka							
	ss1	ss2	ss3	ss4	ss5	ss6	ss7	ss8
SiO ₂	40.5	40.5	40.6	39.3	33.6	32.5	32.1	32.1
Al ₂ O ₃	— ²	—	—	—	.12	.05	.06	.16
Cr ₂ O ₃	.06	.05	.07	.06	—	.14	.13	.05
FeO	10.9	9.8	10.8	16.1	47.5	56.4	57.6	56.9
MnO	.26	.27	.17	.26	.37	.51	.52	.57
MgO	48.1	49.2	48.2	44.1	17.7	10.0	9.25	9.61
CaO	.09	.10	.09	.10	.16	.07	—	.11
NiO	—	.09	—	—	.41	.25	.21	.42
Total	99.9	100.0	99.9	99.9	99.9	99.9	99.9	99.9
X _{Fe} ¹	.113	.100	.112	.170	.601	.760	.777	.769

¹: Fe/(Mg+Fe), ²: not detected.

*Fig. 10.*

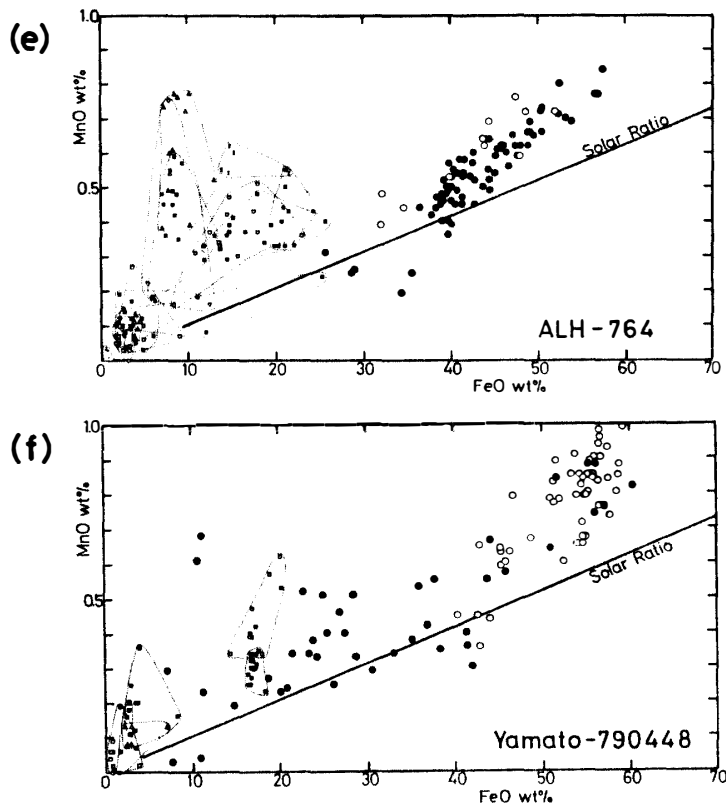


Fig. 10. MnO vs. FeO variations in matrix olivine of six primitive type-3 ordinary chondrites (solid circles). Those of chondrule olivines (various small marks) and Fe, Al-rich materials (open circles) are also plotted in the same diagram. (a) Krymka, (b) Chainpur, (c) Sharps, (d) Tieschitz, (e) ALH-764 and (f) Yamato-790448.

much higher than that in matrix ferrous olivine. Since the compositional ranges of magnesian matrix olivine ($Fa_{<30}$), as shown in the FeO-MnO plots, significantly overlap those of chondrule olivine, it is suggested that most of magnesian olivine in opaque matrix would have been derived from chondrule or chondrule fragments.

The individual micron-sized grain of ferrous olivine in matrices is sometimes chemically zoned (Figs. 1, 3 and 6). Representative analyses for several core-rim pairs of micron-sized matrix olivine are tabulated in Table 4 and the FeO and MnO contents of these pairs are plotted in Fig. 11. The cores of these zoned olivine grains are relatively magnesian (Fa_{11-41}). The rims are enriched in FeO (Fa_{49-67}). With the increase of FeO contents from the cores to the rims, the MnO contents also increase remarkably. The MnO and FeO contents obtained by step scanning for a matrix olivine with an anomalously asymmetrical zoning in Krymka (Fig. 1) are also plotted in Fig. 11. The MnO/FeO ratios through step scanning from core to rim appear to be kept nearly to solar ratio.

3.2. Pyroxenes

Both Ca-poor and Ca-rich pyroxenes are generally present in matrices and rims from meteorite samples studied here. These pyroxenes occur as micron-sized sub-round to angular grains in opaque matrix. Representative analyses of pyroxenes are

Table 5. Representative analyses of matrix pyroxene in four primitive type-3 ordinary chondrites: Sharps (H3.4), Chainpur (LL3.4), ALH-764 (LL3.3), and Yamato-790448 (LL3). These data were obtained by the WDA. Apparent diameter of pyroxene grain (D) is also listed.

Meteorite												
Sharps												
SiO ₂	58.4	57.2	57.7	56.2	55.9	55.5	53.1	52.5	54.5	49.9	53.3	51.6
TiO ₂	— ²	.06	—	—	.11	—	—	.07	.13	.48	.30	.55
Al ₂ O ₃	.05	.34	.33	.33	.80	.43	.21	.58	1.45	7.10	.88	2.36
Cr ₂ O ₃	.32	.50	.59	.71	.83	.90	.82	.42	2.13	1.25	1.67	.90
FeO	1.45	3.04	4.55	7.87	7.28	12.1	21.4	21.8	7.60	9.22	9.11	15.3
MnO	.06	.23	.28	.42	1.08	.63	.73	.30	1.96	.34	.85	.70
MgO	39.0	37.9	36.2	34.0	31.4	28.7	22.5	22.9	27.3	21.4	15.6	12.3
CaO	.04	.22	.30	.30	2.87	1.64	1.13	1.26	4.65	10.6	18.4	15.1
Na ₂ O	—	—	.10	.07	.11	.07	.08	.07	.08	.11	.71	.88
Total	99.3	99.5	100.1	99.9	100.4	100.0	100.0	99.9	99.8	100.4	100.8	99.7
X _{Fe} ¹	.020	.043	.066	.115	.115	.191	.348	.349	.135	.195	.247	.411
Wo	0.1	0.4	0.5	0.6	5.5	3.2	2.3	2.5	9.6	22.4	39.0	34.2
Fs	2.0	4.3	6.5	11.4	10.9	18.5	34.0	34.0	12.2	15.1	15.1	27.0
En	97.9	95.3	93.0	88.0	83.6	78.3	63.7	63.5	78.2	62.5	45.9	38.8
D [μ m]	7	5	6	6	4	3	6	3	5	3	6	3
Meteorite												
Chainpur												
SiO ₂	58.6	57.8	56.5	56.4	55.3	56.1	54.1	52.4	53.4	51.4	52.1	51.7
TiO ₂	.09	—	.15	.06	.13	.05	—	.08	—	.21	1.40	.28
Al ₂ O ₃	.49	.31	1.48	.55	1.34	.74	.21	1.07	.43	6.05	2.35	.95
Cr ₂ O ₃	.94	.68	.82	.69	.28	.79	.69	.61	.53	.88	.77	1.76
FeO	1.90	2.76	3.13	7.02	6.95	8.01	16.1	16.9	16.9	10.6	13.4	8.67
MnO	.40	.28	.80	.53	.12	.75	.70	.64	.88	.49	.43	.48
MgO	38.5	37.7	34.1	33.2	33.2	32.0	27.3	26.6	26.1	23.7	23.8	16.7
CaO	.36	.37	2.45	1.28	2.38	1.81	.69	1.19	1.37	5.10	5.79	18.8
Na ₂ O	—	.06	.10	.09	.22	.07	.23	.37	.33	1.51	—	.62
Total	101.3	100.0	99.5	99.8	99.9	100.3	100.0	99.9	99.9	99.9	100.1	100.0
X _{Fe} ¹	.027	.039	.049	.106	.105	.123	.249	.263	.266	.201	.240	.225
Wo	0.6	0.7	4.7	2.4	4.4	3.4	1.3	2.3	2.7	11.0	11.7	38.5
Fs	2.7	3.9	4.7	10.3	10.1	11.9	24.6	25.6	25.9	17.9	21.2	13.9
En	96.7	95.4	90.6	87.3	85.5	84.7	74.1	72.0	71.4	71.1	67.1	47.6
D [μ m]	19	9	5	3	7	4	4	4	6	4	10	5

Table 5 (continued).

Meteorite	ALH-764											
SiO ₂	59.1	58.5	56.9	55.2	55.8	54.5	56.0	52.7	49.4	53.1	51.5	52.9
TiO ₂	— ²	—	.19	.08	—	.12	—	.23	.64	.36	—	—
Al ₂ O ₃	—	.18	1.19	.40	.13	1.74	.28	1.07	2.23	1.44	5.63	6.12
Cr ₂ O ₃	.15	.54	.65	1.03	.41	1.28	.55	.57	.49	1.96	.17	1.02
FeO	1.97	2.82	5.23	7.57	12.1	10.7	13.8	20.9	23.1	7.61	13.9	9.99
MnO	—	.12	.28	.61	.52	.17	.31	.34	.45	.63	.16	.24
MgO	38.5	37.6	34.2	31.9	29.5	28.9	27.8	22.0	17.3	17.5	12.8	12.1
CaO	.17	.18	.70	3.00	.30	1.70	.90	2.24	6.28	16.3	14.2	15.0
Na ₂ O	—	—	.25	.12	.05	—	.25	—	—	1.16	1.32	2.23
Total	99.9	99.9	99.6	99.9	98.8	99.1	99.9	100.1	99.9	100.1	99.7	99.6
X _{Fe} ¹	.028	.040	.079	.118	.187	.172	.217	.347	.428	.197	.379	.316
Wo	0.3	0.3	1.3	5.6	0.6	3.4	1.8	4.6	13.0	35.0	33.1	37.9
Fs	2.8	4.0	7.8	11.1	18.6	16.6	21.3	33.2	37.3	12.8	25.4	19.6
En	96.9	95.7	90.9	83.3	80.8	80.0	76.9	62.3	49.7	52.2	41.5	42.5
D [μm]	4	7	4	6	13	3	3	7	4	2	3	2
Meteorite	Yamato-790448											
SiO ₂	59.2	58.0	57.1	56.5	54.6	55.1	54.4	54.0	52.9			
TiO ₂	.06	.07	.06	.08	—	.29	.40	.59	—			
Al ₂ O ₃	.37	.83	.38	.75	.26	1.55	1.85	2.26	5.45			
Cr ₂ O ₃	.62	.34	.81	.90	3.38	.92	1.61	1.88	.06			
FeO	1.73	2.38	6.15	4.03	8.55	9.94	2.46	3.77	17.7			
MnO	.43	.19	.53	1.36	1.92	.36	1.78	.81	.33			
MgO	37.1	36.2	34.4	32.9	28.0	27.7	20.5	18.3	11.8			
CaO	.46	1.75	.43	3.43	1.88	4.02	16.7	17.8	9.28			
Na ₂ O	.05	.09	—	—	1.22	—	.20	.48	1.95			
Total	100.0	99.9	99.9	100.0	99.8	99.9	99.9	99.9	99.5			
X _{Fe} ¹	.026	.035	.091	.064	.146	.168	.063	.103	.457			
Wo	0.9	3.2	0.8	6.5	4.0	8.0	35.4	38.4	23.5			
Fs	2.5	3.4	9.0	6.0	14.0	15.4	4.1	6.4	35.0			
En	96.6	93.4	90.2	87.5	82.0	76.6	60.5	55.2	41.5			
D [μm]	7	4	12	6	3	7	5	8	3			

¹: Fe/(Mg+Fe), ²: not detected.

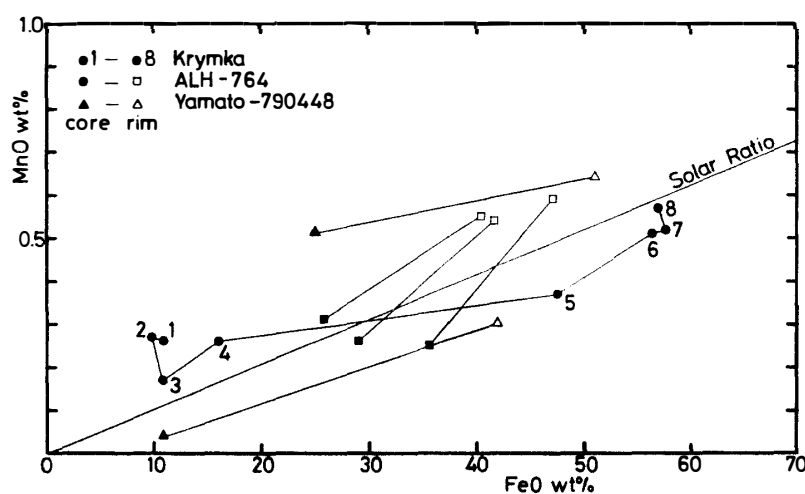


Fig. 11. MnO vs. FeO variations of matrix olivine with compositional zoning in Krymka, ALH-764 and Yamato-790448 chondrites. From core to rim, the MnO content increases with the FeO content.

listed in Table 5. Average and 1σ of chemical composition and grain size of Ca-poor and Ca-rich pyroxenes are tabulated in Table 6. Most Ca-poor pyroxene grains are characterized by low X_{Fe} (0.01–0.20), but some Ca-poor pyroxenes are more iron-rich as much as ~ 0.37 . The compositions of matrix pyroxenes are plotted on the Ca-Mg-Fe diagram (Fig. 12). The range of pyroxene composition observed in the matrix and rims is very wide. The Ca-Mg-Fe ratios of Ca-poor pyroxene range in $Wo_{0-8}Fs_{1-34}En_{62-95}$; those of Ca-rich pyroxene range in $Wo_{8-39}Fs_{4-37}En_{39-78}$. Ca-rich pyroxene in matrices is much less abundant than Ca-poor magnesian pyroxene. In general, matrix Ca-rich pyroxenes are enriched in Fe, Ca, Al, Ti, Cr, Mn and Na relative to more Ca-poor, magnesian ones (Table 5). In Ca-poor pyroxene, the concentrations of minor elements are <0.4 wt% TiO_2 , <3.9 wt% Al_2O_3 , 0.1–3.4 wt% Cr_2O_3 , <2.8 wt% MnO, <4.0 wt% CaO, and <1.4 wt% Na_2O . On the other hand, Ca-rich pyroxenes contain <1.4 wt% TiO_2 , 0.5–13.1 wt% Al_2O_3 , <2.0 wt% Cr_2O_3 , 0.1–2.0 wt% MnO, 4.0–18.8 wt% CaO, and <2.7 wt% Na_2O .

3.3. Sodic plagioclase-like and Ca, Al-rich materials

Representative or average compositions of sodic plagioclase from recrystallized matrix of ALH-77216, albite-like materials of Tieschitz “white matrix” and Si, Al-rich materials of Y-790448 matrix are tabulated in Table 7. Average compositions of Ca, Al-rich materials in matrix of ALH-764 are also listed in Table 7. In the recrystallized matrix and chondrule rims of ALH-77216, sodic plagioclase ($Or_7Ab_{92}An_1$) usually occurs as interstitial grain among granular olivine and low-Ca pyroxene and in contact with larger metallic Fe-Ni, troilite and silicate grains. Sodic plagioclase contains small amounts (generally <1 wt% each) of FeO and MgO. In opaque matrix sodic plagioclase appears to be absent at the scale of SEM images. Interstitial spaces of matrix of ALH-77216, Mezö-Madaras and ALH-77214 are frequently filled with possibly amorphous materials. Average compositions of these uncharacterized, interstitial materials of ALH-77216, Mezö-Madaras and ALH-77214 chondrites are also listed

Table 6. Average compositions and grain size of Ca-poor and Ca-rich pyroxenes in matrix of Sharps, Chainpur, ALH-764 and Yamato-790448 chondrites, obtained by WDA.

Meteorite	Sharps				Chainpur			
	Ca-poor px		Ca-rich px		Ca-poor px		Ca-rich px	
	mean	1 σ	mean	1 σ	mean	1 σ	mean	1 σ
N	38		8		13		6	
SiO ₂	57.1	1.4	52.4	1.7	55.6	1.7	52.7	1.3
TiO ₂	.09	.08	.38	.13	.06	.04	.61	.63
Al ₂ O ₃	.52	.38	3.94	4.23	.62	.43	2.57	1.97
Cr ₂ O ₃	.60	.21	1.31	.52	.63	.23	1.03	.57
FeO	5.00	4.81	8.98	3.39	8.30	5.26	11.7	2.0
MnO	.34	.27	.82	.53	.50	.24	.51	.18
MgO	35.4	4.0	18.6	4.9	33.0	4.0	21.1	4.6
CaO	.78	.78	12.9	4.7	1.05	.78	9.19	5.75
Na ₂ O	.06	.04	.63	.53	.14	.12	.52	.56
K ₂ O	— ²		—		—		—	
Total	99.9		100.0		99.9		99.9	
X _{Fe} ¹	.073	.078	.213	.103	.124	.083	.236	.053
Wo	1.5		28.2		2.0		19.3	
Fs	7.2		15.3		12.1		19.1	
En	91.3		56.5		85.9		61.7	
D [μ m]	4.8	2.1	3.9	1.2	6.0	4.2	7.5	3.3

Meteorite	ALH-764				Yamato-790448			
	Ca-poor px		Ca-rich px		Ca-poor px		Ca-rich px	
	mean	1 σ	mean	1 σ	mean	1 σ	mean	1 σ
N	18		13		36		4	
SiO ₂	56.4	1.6	52.6	1.5	57.0	1.6	53.3	1.1
TiO ₂	.08	.07	.17	.18	.06	.05	.26	.28
Al ₂ O ₃	.59	.51	3.41	2.66	.60	.67	3.72	1.94
Cr ₂ O ₃	.72	.33	1.02	.48	.69	.49	.89	1.00
FeO	8.42	5.49	12.0	4.2	4.94	2.98	10.5	8.6
MnO	.35	.19	.38	.18	.38	.36	.83	.67
MgO	32.3	4.6	17.1	5.0	35.2	2.8	15.6	4.5
CaO	.97	.88	11.9	3.1	.84	.93	13.1	4.8
Na ₂ O	.11	.10	1.19	.91	.12	.30	1.12	.91
K ₂ O	— ²		.15	.16	—		.30	.35
Total	99.9		99.9		99.8		99.6	
X _{Fe} ¹	.128	.092	.283	.090	.073	.047	.275	.218
Wo	1.8		26.4		1.6		30.5	
Fs	12.5		20.9		7.2		19.1	
En	85.6		52.8		91.3		50.5	
D [μ m]	6.3	3.8	3.2	1.3	7.6	4.9	4.6	2.4

¹: Fe/(Mg + Fe), ²: not detected.

in Table 7. The compositions are generally enriched in SiO₂ (52–69 wt%), Al₂O₃ (10.6–21.9 wt%) and alkalis (3.9–12.3 wt% Na₂O, <3.41 wt% K₂O, 0.2–8.1 wt% CaO). They also contain small amounts of FeO (0.7–13.3 wt%), MgO (<12.6 wt%) and

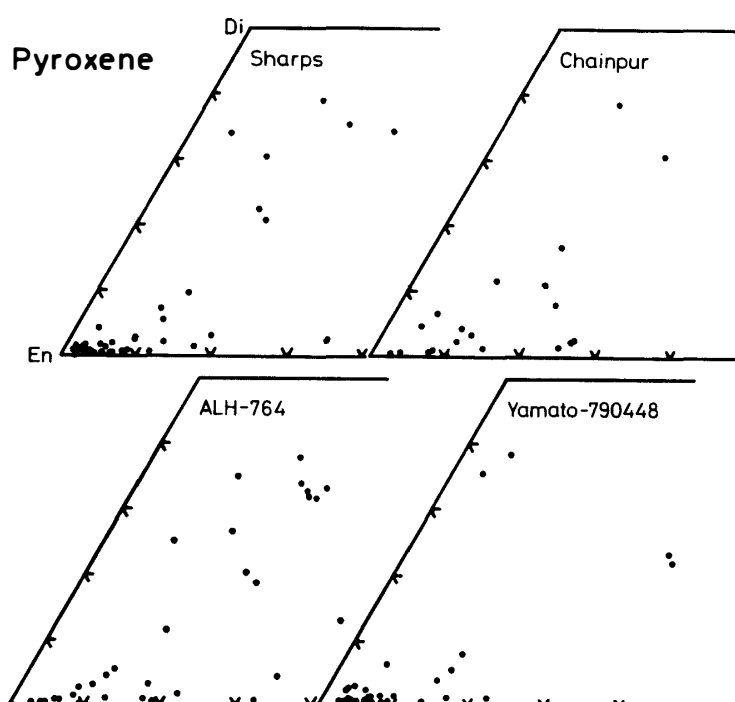


Fig. 12. Chemical compositions of pyroxenes in matrices of four primitive type-3 ordinary chondrites: Sharps, Chainpur, ALH-764 and Yamato-790448.

P_2O_5 (<1.7 wt%). On the other hand, albite-like materials of Tieschitz matrix usually occur as micron-sized, single grains. Si, Al-rich materials in matrix of Y-790448 are commonly enclosed by thin rinds of aggregates composed of Fe, Al-rich materials (Fig. 13). Their chemical compositions are similar to those of interstitial materials: in ab-like materials of Tieschitz, 54–63 wt% SiO_2 , 17–21 wt% Al_2O_3 , 0.7–8.8 wt% FeO, 1.0–6.6 wt% MgO, 0.6–5.0 wt% CaO, 9.8–13.0 wt% Na_2O and <0.6 wt% K_2O ; in Si, Al-rich materials of Y-790448, 56–78 wt% SiO_2 , 5.7–25 wt% Al_2O_3 , 1.5–27 wt% FeO, 0.5–11 wt% MgO, 0.1–3.9 wt% CaO, 0.5–5.3 wt% Na_2O and 0.5–1.9 wt% K_2O . Ab-like materials have already been described by CHRISTOPHE MICHEL-LÉVY (1976) and NAGAHARA (1984).

Ca, Al-rich materials are rarely observed in opaque matrix of ALH-764 chondrite. They occur as aggregates of micron-sized grains with thin FeO-rich rimming materials. The compositions are characterized by higher contents of CaO (as much as ~15 wt%) than those of the above Ab-component-rich materials: 53–57 wt% SiO_2 , 6–7.8 wt% Al_2O_3 , 8.4–13.8 wt% FeO, 9.5–11.3 wt% MgO, 13.1–15.3 wt% CaO, 0.8–1.8 wt% Na_2O and ~0.5 wt% K_2O . It seems that they are one of Ca, Al-rich components of opaque matrix in UOCs as well as Ca-rich pyroxenes.

3.4. Fe, Al-rich materials

Generally, matrices and rims in UOCs commonly contain micron-sized, Fe, Al-rich particles. These materials appear to be homogeneous and possibly amorphous at the scale of SEM images, although they are still uncharacterized in detail. NAGAHARA (1984) has described similar Fe, Al-rich materials in the opaque matrix of Semar-

Table 7. Representative analyses of plagioclase and average compositions of plagioclase-like, Al-rich phases in matrix (normalized to 100 wt%), obtained by SEM-EDS and WDS analyses.

Meteorite	Chainpur anorthite	ALH-77216 albite	Tieschitz Ab-like material		Y-790448 Si, Al-rich material ¹		ALH-764 Ca, Al-rich material ¹	
			39	1 σ	15	1 σ	5	1 σ
N			mean	1 σ	mean	1 σ	mean	1 σ
SiO ₂	45.0	68.2	59.3	2.0	69.7	6.2	55.8	1.7
TiO ₂	— ²	—	.17	.14	.23	.22	—	—
Al ₂ O ₃	33.7	18.5	18.6	.9	14.0	5.1	7.33	.8
Cr ₂ O ₃	—	—	.09	.08	.09	.17	.25	.05
FeO	1.87	.96	4.46	1.78	7.23	6.85	10.3	2.3
MnO	—	—	.09	.08	.12	.13	.14	.03
MgO	—	—	2.76	1.17	3.78	3.12	10.1	.8
CaO	18.6	.22	2.66	.91	1.09	.87	14.5	1.0
Na ₂ O	.52	10.4	11.5	.9	2.28	1.62	1.08	.40
K ₂ O	—	1.15	.29	.13	1.14	.45	.52	.02
P ₂ O ₅	—	—	.14	.29	—	—	—	—
NiO	—	—	—	—	.31	.37	—	—
Or	.0	6.7						
Ab	4.7	92.2						
An	95.3	1.1						

Meteorite	Mezö-Madaras interstices		ALH-77216 interstices		ALH-77214 interstices	
	9	1 σ	16	1 σ	4	1 σ
N	mean	1 σ	mean	1 σ	mean	1 σ
SiO ₂	60.8	4.3	62.0	4.5	62.3	3.4
TiO ₂	.47	.12	.08	.13	.30	.13
Al ₂ O ₃	14.1	2.1	18.1	2.6	16.9	3.4
Cr ₂ O ₃	.22	.20	.13	.24	— ²	—
FeO	5.80	3.58	5.03	3.60	4.03	1.19
MnO	.26	.16	.06	.07	.14	.15
MgO	6.52	3.41	1.89	2.26	2.70	.88
CaO	3.68	2.30	2.58	2.27	4.08	1.97
Na ₂ O	7.54	2.69	8.22	1.28	9.20	1.06
K ₂ O	.34	.18	1.04	.82	.10	.02
P ₂ O ₅	.14	.23	.27	.43	.13	.25
NiO	.12	.13	.63	.81	.12	.09

¹: obtained by WDA, ²: not detected.

kona chondrite and called them “fluffy particles”. Using STEM, IKEDA *et al.* (1981) have showed that the amorphous material in the matrix of ALH-77015 is glass and is the main constituent of the matrix. Typical occurrences of Fe, Al-rich materials in opaque matrix are shown in Figs. 13 and 14. Representative occurrences suggesting their formation processes observed in opaque matrix are classified into the following three types: (1) subround to angular single grain, (2) fine-grained aggregate overgrown on enstatite and (3) fine-grained aggregate overgrown on Si, Al-rich materials.

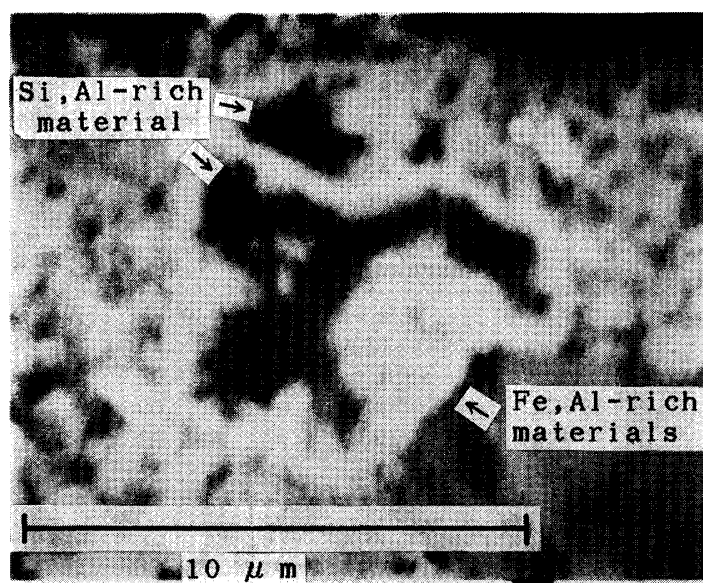


Fig. 13. SEM photograph of Fe, Al-rich materials (light) overgrown on Si, Al-rich materials (dark) in Yamato-790448 matrix. The boundary between the two is irregular.

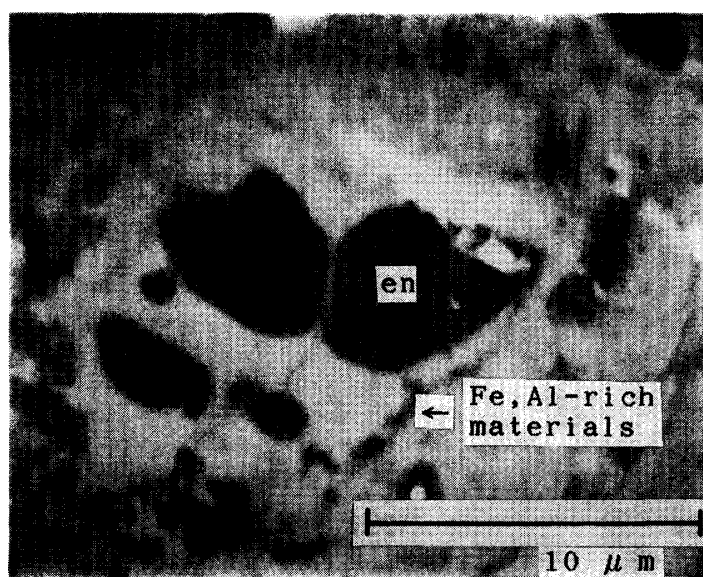


Fig. 14. SEM photograph of Fe, Al-rich materials overgrown on enstatite grains in Yamato-790448 matrix.

Figure 13 shows Fe, Al-rich materials overgrown on Si, Al-rich materials of Y-790448 matrix. The boundary between the two is irregular, suggesting that the Si, Al-rich material would have reacted with Fe-rich fluid to form the Fe, Al-rich, fine-grained aggregate rimming it. Figure 14 shows Fe, Al-rich materials overgrown on matrix enstatite grains. The thickness is not uniform and the boundary is generally smooth.

As shown for sodic plagioclase-like materials, the Fe, Al-rich materials also have variable compositions similar to mixtures of sodic plagioclase and ferrous olivine. In contrast to the former, the composition of the latter is generally enriched in MgO and

Table 8. Average compositions of Fe, Al-rich materials in matrix (normalized to 100 wt%), obtained by SEM-EDS and WDS methods. Average grain size (D) is also listed.

Meteorite	Semarkona		single grain	+En	+Metal	Krymka		Tieschitz	Sharps		Chainpur		ALH-764		Yamato-790448	
	Fe, Al-rich material ¹					Fe, Al-rich material	Fe, Al-rich material	Fe, Al-rich material								
	31	19				2	1	4		5		11		53		
N	mean	1σ	mean	mean	mean	1σ		mean	1σ	mean	1σ	mean	1σ	mean	1σ	
SiO ₂	45.5	4.0	45.8	42.9	51.1	33.8	1.1	37.0	34.2	.8	35.7	2.5	35.8	2.6	35.0	1.8
TiO ₂	.11	.14	.12	.10	—	.06	.05	—	.06	.04	.11	.08	—	—	—	—
Al ₂ O ₃	5.25	3.74	5.94	3.89	4.98	3.22	2.08	2.28	2.48	.37	1.86	1.17	2.88	1.06	1.07	1.13
Cr ₂ O ₃	.31	.49	.19	.15	1.50	.16	.04	—	.17	.16	.20	.17	.37	.40	.10	.13
FeO	34.5	9.6	32.5	44.7	17.0	48.5	9.1	42.6	42.5	.6	40.9	5.6	42.4	6.9	52.6	5.5
MnO	.38	.52	.33	.16	1.35	.46	.15	.57	.55	.02	.57	.12	.60	.12	.76	.16
MgO	9.70	5.69	10.6	4.04	21.2	11.6	4.67	16.9	19.0	.7	20.0	4.1	16.4	3.8	9.52	4.10
CaO	.82	1.10	.97	.60	.52	.83	.46	.28	.33	.33	.39	.63	.29	.42	.24	.12
Na ₂ O	2.74	.95	2.84	2.97	1.42	.75	.17	.28	.48	.12	.21	.12	.94	.34	.21	.19
K ₂ O	.65	.34	.76	.47	.55	.18	.18	.06	.15	.04	.06	.04	.15	.08	.06	.06
P ₂ O ₅	.07	.13	—	.08	.40	—	—	—	—	—	—	—	—	—	—	—
NiO	— ³	—	—	—	—	.44	.47	—	.17	.10	.06	.10	.15	.17	.45	.30
X _{Fe} ²	.666	.184	.633	.861	.311	.700	.124	.587	.556	.010	.534	.079	.592	.093	.756	.093
D [μm]	6.5	2.5	7.0	6.1	5.7	4.6	.1	7	4.5	1.6	6.8	4.3	3.9	.8	4.7	2.1

¹: obtained by SEM-EDS method, ²: Fe/(Mg+Fe), ³: not detected.

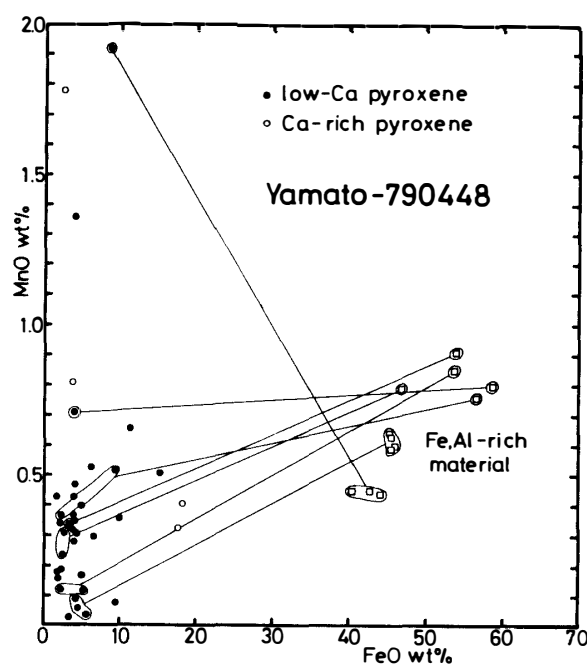


Fig. 15. MnO vs. FeO variations of pyroxenes and the Fe, Al-rich materials overgrown on pyroxenes in Yamato-790448 matrix. The corresponding value of the latter coexisting with the former is connected with tie line.

FeO and poorer in SiO_2 , Al_2O_3 and Na_2O . However, the Al_2O_3 contents vary widely as much as ~ 14 wt%. Average compositions and grain size of Fe, Al-rich materials in opaque matrix are tabulated in Table 8. The Fe, Al-rich material is characterized by the composition similar to mixture of a large amount of ferrous olivine component and a small amount of sodic plagioclase component. Fe, Al-rich materials frequently contain significant amounts of Al_2O_3 (as much as ~ 7.5 wt%) and Na_2O (as much as ~ 1.6 wt%). Similarly, the Cr_2O_3 and NiO contents are sometimes high as much as ~ 1.3 wt%. The high NiO content may be due to tiny inclusion of metallic Fe-Ni. They commonly contain a significant amount of MnO as much as 1.0 wt%. Especially, the MnO content increases remarkably with increasing FeO content (Fig. 10a-f) as well as ferrous olivine in opaque matrix. In the case of Fe, Al-rich materials overgrown on matrix enstatite, it is revealed that the MnO content shows no clear correlation with that of the inner pyroxene grain (Fig. 15). In Semarkona, Fe, Al-rich materials show remarkable variations of composition with different types of occurrence. As shown in Fig. 8, single Fe, Al-rich materials show a wide variation of X_{Fe} , ranging from 0.42 to 0.82. In the case of Fe, Al-rich materials coexisting with enstatite, they are characterized by higher X_{Fe} (0.74–0.92). On the other hand, Fe, Al-rich materials coexisting with Fe-Ni metals have low X_{Fe} (0.28–0.33). Recently, HUTCHISON *et al.* (1987) and ALEXANDER *et al.* (1989b) have showed that some of FeO-rich materials are composed of smectite or 'fayalitic' material and its alteration products in matrix and rims of Semarkona. Since some of Fe, Al-rich materials of this study is similar to Semarkona smectite in composition (Table 8), it is reasonable that they formed as alteration products during aqueous alteration of Si, Al-rich matrix materials (Fig. 13).

3.5. Silica-rich spherules

Spherules composed mainly of highly SiO_2 -rich, uncharacterized materials are

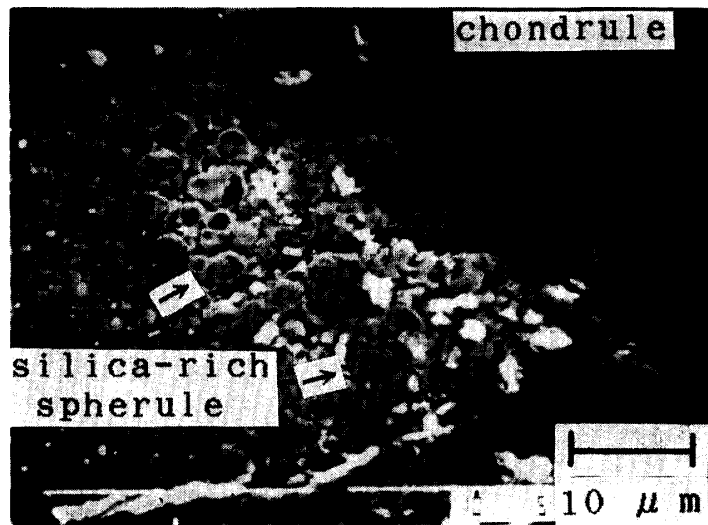


Fig. 16. SEM photograph of silica-rich spherules in a chondrule rim of Chainpur. Micron-sized silica-rich spherules are rimmed with thin rinds of ferrous olivine or pyroxene.



Fig. 17. SEM photograph of silica-rich spherules in a chondrule rim of Sharps.

rarely observed in chondrule rims of Chainpur and Sharps and opaque matrix in Sharps (Figs. 5, 16 and 17). These spherules commonly have thin rinds of ferrous olivine or Fe-rich, low-Ca pyroxene. Thickness of the rind is typically 2–4 μm . Representative and average analyses of silica-rich spherules are shown in Table 9. Their chemical compositions are characterized by high SiO_2 content (76–93 wt%), and low Al_2O_3 (<1.8 wt%), MgO (1.2–8.8 wt%), FeO (3.9–14.7 wt%), CaO (<3.9 wt%), Na_2O and K_2O (<0.2 wt%) contents. The FeO-MnO relations of silica-rich spherule and coexisting olivine and pyroxene are plotted in Fig. 18. Generally, the MnO content of silica-rich spherule is low (<0.3 wt%). The coexisting olivine or pyroxene has high MnO content ranging from 0.33 to 0.7 wt%. It seems impossible to explain the FeO-MnO relation by solid-solid reaction between silica-rich spherules and Fe-Ni metals.

Table 9. Representative analyses and average composition of silica-rich spherules in matrices and rims of Sharps and Chainpur chondrites, obtained by WDS analysis (normalized to 100 wt%). Grain diameter and mean grain size (D) are also listed.

Meteorite	Sharps					Chainpur			Average $N=8$	1σ
SiO ₂	92.4	75.8	92.3	92.9	85.8	78.7	79.7	81.5	84.9	6.9
TiO ₂	— ¹	.05	—	—	—	—	.09	.05	—	
Al ₂ O ₃	.23	.19	.19	—	—	.32	1.81	.22	.37	.59
Cr ₂ O ₃	—	—	—	—	.05	.20	.17	.15	.07	.09
FeO	4.86	14.7	3.86	5.20	10.8	11.4	7.02	9.69	8.44	3.80
MnO	.07	.28	.13	.08	.19	.18	.23	.20	.17	.07
MgO	1.23	4.95	1.53	1.72	3.08	8.65	8.81	7.87	4.73	3.30
CaO	.88	3.86	1.79	—	—	.34	1.86	.12	1.11	1.34
Na ₂ O	.16	.14	.12	—	—	.22	.14	.13	.12	.07
K ₂ O	—	—	—	—	—	.05	.07	—	—	
NiO	.09	.07	—	.06	—	—	.07	.05	.05	.03
D (μm)	4		2	4		2	3	2	2.7	1.2

¹: not detected.

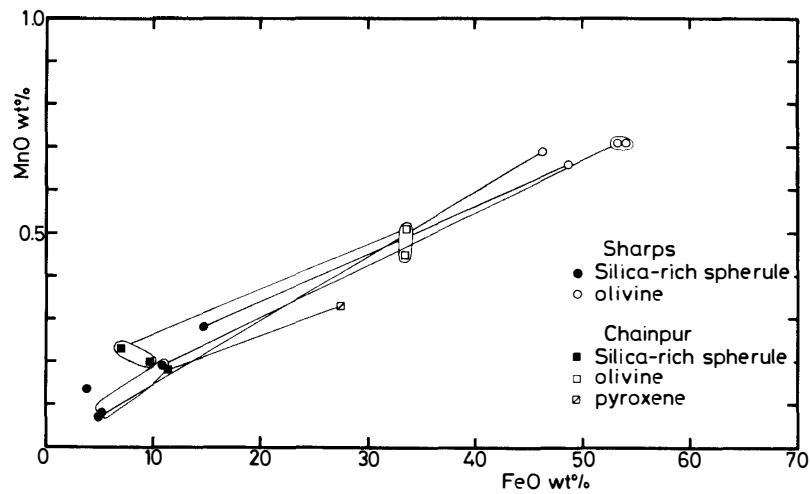


Fig. 18. MnO vs. FeO variations of silica-rich spherules and the coexisting olivine and pyroxene in matrices and rims of Chainpur and Sharps.

3.6. Opaque minerals

In opaque matrix, micron-sized grains of Fe-Ni metals and troilite frequently occur. In the matrix of Semarkona chondrite, magnetite crystals are commonly observed. Especially, tiny magnetite crystals are present in several chondrule rims of Semarkona. Average composition of magnetite grains in Semarkona is 92.7 FeO wt%, <0.05 MnO wt%, 0.17 NiO wt% and 0.05 Cr₂O₃ wt% (number of averaged analyses is 12). It is to be noted that the MnO contents of these magnetite grains are extremely low.

3.7. Other minerals

Anorthite crystals (Ab₅An₉₅, a few μm in diameter) rarely occur as tiny angular

fragments in opaque matrix of Chainpur. Accessory calcite and spinel crystals are rarely found in Semarkona matrix (NAGAHARA, 1984; MATSUNAMI, 1984). Representative analyses of these minerals are MgO 26.9 wt%, FeO 6.38 wt%, Al₂O₃ 66.1 wt%, Cr₂O₃ 0.30 wt%, MnO 0.12 wt%, for spinel, and CaO 53.9 wt%, FeO 1.16 wt%, <0.05 MnO wt%, MgO 0.88 wt%, CO₂ 44.1 wt%, for calcite, respectively. Whitlockite crystal was identified in "white matrix" of Tieschitz (CaO 45.7 wt%, P₂O₅ 46.4 wt%, FeO 1.66 wt%, MgO 3.43 wt%, Na₂O 2.59 wt% and K₂O 0.28 wt%).

3.8. Aggregate of submicron-sized grains

Besides Fe, Al-rich materials, aggregates of submicron-sized grains are also included in the matrices. These aggregates appear to be consisting of submicron-sized silicate grains under SEM. However, they are poorly characterized at the scale of SEM images. These aggregates also show wide variations in chemical composition.

4. Discussion

4.1. Constraints on the formation of matrix olivine in primitive UOCs

For the formation of matrix olivine in primitive type-3 chondrites several hypotheses have been proposed by many authors. These can be classified into the following five categories: (1) regolith origin (*e.g.*, RAMBALDI *et al.*, 1981; ALEXANDER *et al.*, 1989a), (2) products of solid-solid reactions between enstatite, silica and metallic Fe-Ni at low temperatures (HOUSLEY and CIRLIN, 1983; NAGAHARA, 1984; NAGAHARA and KUSHIRO, 1987), (3) products of solid-gas reactions between metallic Fe and silica-rich gas (NAGAHARA, 1984; NAGAHARA and KUSHIRO, 1987), (4) products of solid-gas reactions among enstatite, metallic Fe and nebular gas (IKEDA *et al.*, 1981) and (5) direct vapour→solid condensation (KORNACKI and WOOD, 1984; PALME and FEGLEY, 1987; MATSUNAMI *et al.*, 1990). Regolith origin of matrix olivine (1) means that most of matrix olivine were derived as clastic fragments from chondrules or chondrites. The silica saturation assumed in (2) and (3) may be the result of fractional condensation of forsterite from nebular gas (NAGAHARA and KUSHIRO, 1987). ALEXANDER *et al.* (1989a) concluded that most matrix materials were derived from chondrules and considered that matrix fayalitic olivine was formed through the reaction between silica derived from chondrule mesostases, enstatite and metallic Fe. KORNACKI and WOOD (1984) proposed direct condensation model (5) against a formation scheme of matrix olivine predicted in equilibrium condensation theory, based on the mineral chemistry of matrix olivine of the Allende (CV3) chondrite and the sluggishness of solid-solid reactions at low temperatures. In the following sections, we discuss the characteristics of matrix olivine described in the present study in order to reexamine the possibilities of these interpretations on matrix olivine formation.

4.1.1. Formation of matrix magnesian olivine

Among characteristics of composition of matrix olivine, the MnO content is of particular importance. As already shown in Section 3.1, ferrous olivine in opaque matrix commonly contains a significant amount of MnO as much as 1.2 wt%. Particularly, the MnO content of ferrous olivine (Fa_{>~30}) increases remarkably with increasing FeO content (Fig. 10a-f), showing a clear positive correlation of Mn with Fe.

The correlation, however, seems to be not clear in matrix magnesian olivine ($Fa_{<\sim 30}$). The plot largely overlaps on the field of chondrule olivine. Therefore, it is concluded that most of matrix intermediate to Fe-rich olivine cannot be derived as clastic fragments from chondrule olivine ($Fa_{<\sim 40}$; Fig. 7) and that some of matrix magnesian olivine may be clastic fragments from chondrules. In fact, it seems that most grains of matrix magnesian olivine are angular in shape and relatively larger than more ferrous ones, suggesting that this conclusion is reasonable. It may be possible that matrix magnesian olivine with low Mn/Fe ratios would have formed through different mechanisms.

4.1.2. Formation of matrix intermediate olivine

IKEDA *et al.* (1981) suggested the following solid-gas reaction including oxidation of metallic iron: $MgSiO_3(c) + Fe(c) + 1/2 O_2(g) \rightarrow (Mg_{0.5}, Fe_{0.5})_2SiO_4(c)$, where (c) and (g) are crystal and gas phases, respectively. HOUSLEY and CIRLIN (1983) considered that matrix olivine in Allende was formed through the reaction between chondrule enstatite and metallic Fe-Ni during metamorphism of the parent body. NAGAHARA (1984) reported an example of overgrowth of intermediate olivine (Fa_{50}) on magnesian pyroxene (En_{95}) coexisting with metallic Fe-Ni in the matrix of Tieschitz. A similar occurrence of matrix intermediate olivine in Chainpur matrix is shown in Fig. 2. These textural evidences indicate that some of matrix intermediate olivine may be products of reaction between enstatite and metallic Fe-Ni. There are, however, several additional limitations to this interpretation. The reported examples show the fact that grain sizes of intermediate olivine overgrown on enstatite are commonly less than a few μm in diameter, suggesting that single grains of matrix intermediate olivine larger than a few μm may be hardly explained by the above mechanism. Moreover, if we take experimental results of the reaction between enstatite and metallic Fe into consideration (NAGAHARA and KUSHIRO, 1987; MATSUNAMI, 1990), it is to be noted that intermediate olivine must form along the exact boundary between enstatite and metallic Fe-Ni grains. In addition to this, as shown in MATSUNAMI (1990), compositional zoning ranging from $Fa_{\sim 38}$ to $Fa_{\sim 62}$ must be also observed from enstatite/olivine boundary to olivine/metal boundary, unless homogenization of olivine owing to diffusion is appreciable. The case of such occurrence is rare in the matrices of type-3 ordinary chondrites. Furthermore, this argument can be checked by means of mineral chemistry of matrix intermediate olivine. Comparisons of MnO and FeO contents between matrix Ca-poor, magnesian pyroxene, silica-rich spherules of Sharps and Chainpur chondrites and matrix ferrous olivine are shown in Fig. 19. A preliminary result on reaction experiment in a mixture of bronzite (FeO 8.4 wt%, MnO 0.21 wt%) powder and pure Fe powder shows that the MnO contents of formed intermediate olivine (FeO 42.6 wt%, MnO 0.14 wt%) lie just on the tie line connecting bronzite with FeO=100% on the MnO-FeO plot (Fig. 20), if homogenization in formed olivine is effective. For an example shown in Fig. 2, the MnO content of matrix intermediate olivine (FeO 45.3 wt%, MnO 0.49 wt%) overgrown on magnesian pyroxene (FeO 9.52 wt%, MnO 0.43 wt%) is plotted above the tie line. This fact may not fit to the above hypothesis. If we further persist in the validity, we must explain why Mn is highly enriched in olivine. As suggested by LARIMER and ANDERS (1967), it is possible that gaseous $FeCl_2$ would permit formation of FeO-bearing olivine via solid-gas reactions among enstatite,

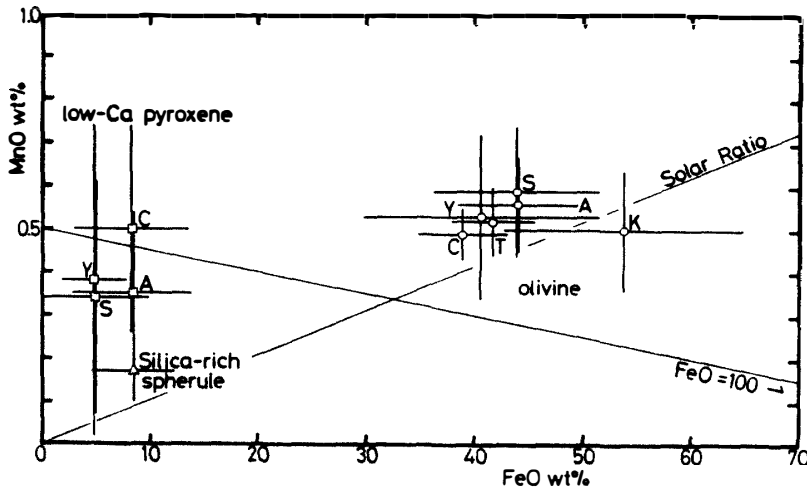


Fig. 19. Comparison of the average MnO and FeO contents of matrix olivine with those of matrix low-Ca pyroxene and silica-rich spherules. Bars denote $\pm 1\sigma$ of these contents. A: ALH-764, C: Chainpur, K: Krymka, T: Tieschitz, S: Sharps, Y: Yamato-790448.

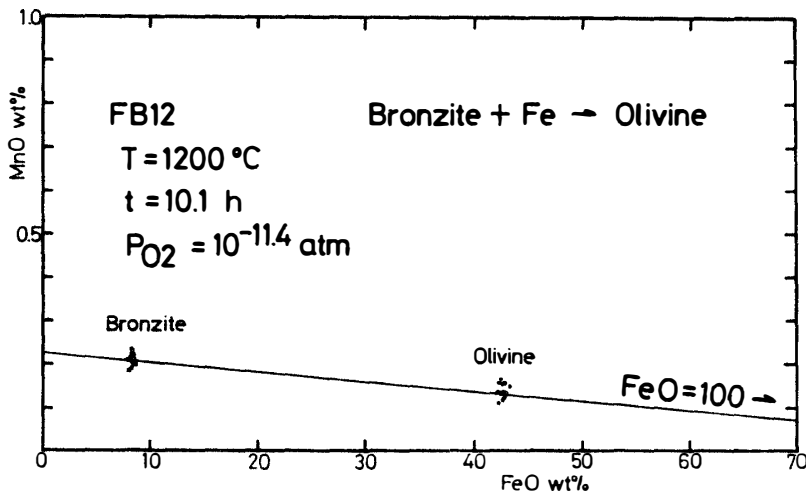


Fig. 20. Comparison of MnO and FeO contents of bronzite (reactant) and intermediate olivine (product), produced through a solid-state reaction in a mixture of bronzite powder and pure metallic Fe powder (FB12: $T=1200^{\circ}\text{C}$; $P_{\text{O}_2}=10^{-11.4}\text{ atm}$; $t=10.1\text{ h}$).

metallic Fe and nebular gas at low temperatures (IKEDA *et al.*, 1981). This mechanism may permit additional Mn to diffuse into intermediate olivine during the solid-gas reaction, although the source of Mn is not clear.

4.1.3. Formation of matrix Fe-rich olivine

Recently, based on detailed observations on matrix of primitive type-3 chondrites and experimental results on the system En-Silica-Metallic Fe ($\pm\text{Fo}$), NAGAHARA (1984) and NAGAHARA and KUSHIRO (1987) have concluded that the silica saturation is necessary to produce matrix Fe-rich olivine. We consider the possibility that solid-solid reactions involving these silicate phases and metallic Fe-Ni can explain various compositional characteristics and mode of occurrence of matrix Fe-rich olivine.

In this paper the existence of micron-sized silica-rich spherules (Figs. 5, 16 and 17)

in opaque matrices and rims of Sharps and Chainpur chondrites has been reported, although these occurrences are not so common in opaque matrix of primitive UOCs. These spherules are enclosed by thin rinds of Fe-rich olivine. The thickness of Fe-rich olivine overgrown on silica-rich spherules is less than 3–4 μm (Fig. 5). The overgrowth texture indicates that silica-rich spherules are closely related to the production of matrix Fe-rich olivine.

As shown in Fig. 19, it is revealed that compositions of matrix ferrous olivine are mainly plotted outside the Ca-poor pyroxene–silica-rich spherule–metallic Fe region. If we accept the solid-solid reaction hypothesis involving silica and take the preliminary result of reaction experiment of bronzite and metallic Fe (Fig. 20) into account, this strongly suggests that matrix Fe-rich olivine would have been formed through reactions involving more Mn-rich pyroxene than those mainly observed in matrix. If matrix Fe-rich olivine were formed by solid-solid reactions involving matrix magnesian pyroxene observed in matrix, we must explain why matrix Fe-rich olivine is relatively enriched in Mn. One possibility is that magnesian, Mn-poor olivine, that would have been simultaneously formed with matrix Fe-rich olivine, might have been lost by an unknown fractionation mechanism.

Furthermore, we must explain a positive correlation of Mn with Fe in matrix ferrous olivine. The MnO/FeO ratios are lower than those of most of chondrule olivine and are distributed around solar ratio (MnO/FeO \sim 0.01) (Fig. 10a–f). Similar tendencies are observed in compositional zoning of matrix ferrous olivine (Fig. 11). The problem is whether this positive correlation is produced by solid-solid reactions between Mn-bearing, magnesian pyroxene, (\pm forsterite), silica-rich spherules and metallic Fe-Ni. One possibility is that the correlation may be produced by diffusion between Mn-poor, magnesian to intermediate olivine and Mn-rich fayalite ($\text{Fa}_{>90}$). Especially, to explain matrix $\text{Fa}_{>90}$ olivine with high enrichment of MnO as much as \sim 0.8 wt%, it is required that very MnO-rich pyroxene as much as \sim 2.0 wt% must be involved in the reactions. However, such Mn-rich, magnesian pyroxene is very scarce in opaque matrix of primitive type-3 ordinary chondrites (see Fig. 15). It is suggested that the positive correlation of Mn with Fe in matrix ferrous olivine cannot be explained by the above solid-solid reactions.

4.2. Implications for matrix formation of primitive type-3 ordinary chondrites

4.2.1. Limitations to solid-solid reaction hypothesis

As already described, textural evidences concerning occurrences of matrix ferrous olivine observed in matrices of primitive type-3 ordinary chondrites seem to indicate that some of matrix ferrous olivine would have been formed through solid-solid reactions between enstatite, (\pm forsterite), silica and metallic Fe-Ni. However, detailed reexaminations of occurrences and mineral chemistry of matrix ferrous olivine suggest that there are several limitations to this hypothesis, although it can explain a wide compositional range of matrix olivine (Fa_{1-96}) (NAGAHARA and KUSHIRO, 1987). The first point is that textural evidences indicate that grain sizes of olivine overgrown on silica-rich spherules or metallic Fe-Ni, formed through this mechanism, are less than 3–4 μm , suggesting that single, matrix ferrous olivine larger than 4 μm is probably impossible to form through this mechanism. The second point is that these reactions

may be incapable of producing strong positive correlation of Mn with Fe in matrix ferrous olivine. Even though this mechanism explains the correlations, the mineral chemistry of matrix magnesian pyroxene, especially the MnO content, must be severely constrained. Thus, it is concluded that this process would have had a relatively minor role in the formation of matrix materials of primitive type-3 ordinary chondrites. Of course, we had to conduct reaction experiments of the Pyroxene-Silica-Fe System on the MnO distribution between Mn-bearing, Mg-rich pyroxene (reactant) and Fe-rich olivine (product) in order to further examine the validity of the solid-solid reaction hypothesis.

KORNACKI and WOOD (1984) suggested that matrix olivine in Allende carbonaceous chondrite would have formed through direct vapour→solid condensation. This mechanism was proposed as an alternative idea to formation of matrix olivine based on equilibrium condensation scheme because of the sluggishness of solid-solid reactions at low temperatures. Recently, PALME and FEGLEY (1987) performed equilibrium calculations to model the formation of FeO-bearing olivine under oxidizing conditions at high temperatures in the solar nebula. They showed that high temperature oxidation in the solar nebula provides a simple means for explaining direct vapour→solid condensation of ferrous olivine.

From the standpoint of non-equilibrium effects of condensation, this mechanism has a significant importance. If Mg is enriched in the condensed olivine and Fe and Mn are relatively enriched to similar extents in the gas phase during non-equilibrium direct vapour→solid condensation, this mechanism may produce both wide variation of Fa mole % and positive correlations of Mn with Fe in condensed olivine. If so, it is possible that matrix ferrous olivine may be the product of the non-equilibrium condensation. However, the validity of this interpretation must be checked theoretically. Recently, MATSUNAMI *et al.* (1990) have presented a simple model of non-equilibrium condensation of (Mg, Fe, Mn)-olivine from a cooling nebular gas to explain a wide compositional variability and a strong positive correlation of MnO with FeO in matrix ferrous olivine of primitive UOCs.

4.2.2. Constraints on $\text{PH}_2\text{O}/\text{PH}_2$ ratio in the formation environments of matrix materials in primitive UOCs

The existence of matrix Fe-rich olivine in primitive UOCs can give clues to understanding the redox state of the nebular gas at the time of formation of matrix ferrous olivine. First, we consider stability limit of (Mg, Fe)-olivine thermodynamically. Figure 21 is a diagram showing lower limits of the $\text{PH}_2\text{O}/\text{PH}_2$ ratios in the gas for stability of (Mg, Fe)-olivine with various compositions at elevated temperatures. The $\text{PH}_2\text{O}/\text{PH}_2$ ratio corresponding to iron-wüstite buffer is also shown. The absence of wüstite in matrices of UOCs indicates that the $\text{PH}_2\text{O}/\text{PH}_2$ ratio of the gas may be lower than that of IW-buffer. Presence of Fa_{98} olivine in Krymka matrix indicates that the ratio may be higher than ~QIF buffer. It is concluded that the ratio is generously constrained to the following range: $0.03 \leq \text{PH}_2\text{O}/\text{PH}_2 \leq 1.0$. This value is $60 \sim 2 \times 10^8$ times larger than that calculated in equilibrium condensation theory (LARIMER and BARTHOLOMAY, 1979: $\sim 5 \times 10^{-4}$). Recently, similar arguments on the redox conditions of the nebular gas have been made by some investigators (WOOD, 1984; FEGLEY and PALME, 1985; PALME and FEGLEY, 1987; RUBIN *et al.*, 1988). They suggested

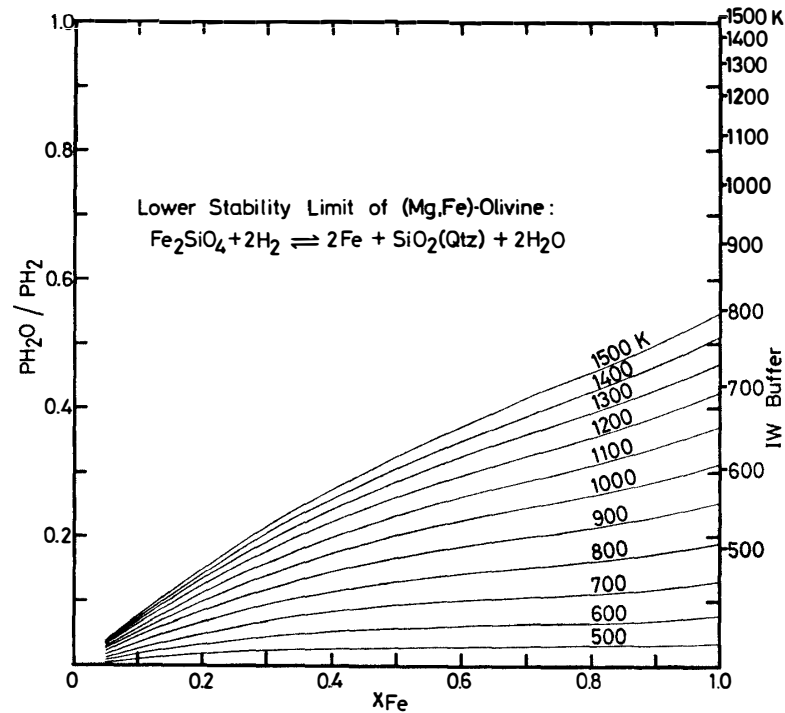


Fig. 21. Lower stability limits of (Mg, Fe)-olivine in terms of $\text{PH}_2\text{O}/\text{PH}_2$ ratios, calculated from thermodynamic data, at elevated temperatures. (Data source: OHMOTO and KERRICK, 1977; MYERS and EUGSTER, 1983; WOOD and KLEPPA, 1981).

relatively higher $\text{PH}_2\text{O}/\text{PH}_2$ ratios of the nebular gas during formation of chondritic materials at high temperatures. From the data of matrix ferrous olivine in UOCs, we can draw similar conclusions.

Next, we consider non-equilibrium effect during direct vapour→solid condensation of matrix ferrous olivine. BLANDER and KATZ (1967) suggested that the supersaturation of the gas phase due to delay of nucleation of metallic Fe-Ni leads to much higher concentrations of FeO in the silicate condensates than those calculated by assuming equilibrium condensation. If their arguments are applicable to the case of non-equilibrium condensation of ferrous olivine crystal, it is also possible that matrix ferrous olivine would have formed through vapour→solid condensation under reducing conditions ($\text{PH}_2\text{O}/\text{PH}_2 \sim 5 \times 10^{-4}$).

Acknowledgments

We are grateful to Prof. I. KUSHIRO and Dr. H. NAGAHARA of the University of Tokyo for valuable suggestions, constructive discussions and encouragement during this work. The helpful reviews by two anonymous referees are also acknowledged. We also thank Drs. K. YOKOYAMA and Y. SAITO of the National Science Museum for permitting S. M. to use the SEM-EDS. We are grateful to Drs. K. YANAI and H. KOJIMA of the National Institute of Polar Research and Dr. B. MASON of the Smithsonian Institution for providing and loaning polished thin sections and meteorite samples.

References

- ALEXANDER, C. M. O., HUTCHISON, R. and BARBER, D. J. (1989a): Origin of chondrule rims and interchondrule matrices in unequilibrated ordinary chondrites. *Earth Planet. Sci. Lett.*, **95**, 187–207.
- ALEXANDER, C. M. O., BARBER, D. J. and HUTCHISON, R. (1989b): The microstructure of Semarkona and Bishunpur. *Geochim. Cosmochim. Acta*, **53**, 3045–3057.
- ALLEN, J. S., NOZETTE, S. and WILKENING, L. L. (1980): A study of chondrule rims and chondrule irradiation records in unequilibrated ordinary chondrites. *Geochim. Cosmochim. Acta*, **44**, 1161–1175.
- ANDERS, E. and EBIHARA, M. (1982): Solar-system abundances of the elements. *Geochim. Cosmochim. Acta*, **46**, 2363–2380.
- ASHWORTH, J. R. (1977): Matrix textures in unequilibrated ordinary chondrites. *Earth Planet. Sci. Lett.*, **35**, 25–34.
- BENCE, A. E. and ALBEE, A. L. (1968): Empirical correction factors for the electron microanalysis of silicates and oxides. *J. Geol.*, **76**, 382–403.
- BLANDER, M. and KATZ, J. L. (1967): Condensation of primordial dust. *Geochim. Cosmochim. Acta*, **31**, 1025–1034.
- BREARLEY, A. J., SCOTT, E. R. D., KEIL, K., CLAYTON, R. N., MAYEDA, T. K., BOYNTON, W. V. and HILL, D. H. (1989): Chemical, isotopic and mineralogical evidence for the origin of matrix in ordinary chondrites. *Geochim. Cosmochim. Acta*, **53**, 2081–2093.
- CHRISTOPHE MICHEL-LÉVY, M. (1976): La matrice noire et blanche de la chondrite de Tieschitz (H3). *Earth Planet. Sci. Lett.*, **30**, 143–150.
- FEGLEY, B., Jr. and PALME, H. (1985): Evidence for oxidizing conditions in the solar nebula from Mo and W depletions in refractory inclusions in carbonaceous chondrites. *Earth Planet. Sci. Lett.*, **72**, 311–326.
- HOUSLEY, R. M. and CIRLIN, E. H. (1983): On the alteration of Allende chondrules and the formation of matrix. *Chondrules and Their Origins*, ed. by E. A. KING. Houston, Lunar Planet. Inst., 145–161.
- HUSS, G. R., KEIL, K. and TAYLOR, G. J. (1981): The matrices of unequilibrated ordinary chondrites; Implications for the origin and history of chondrites. *Geochim. Cosmochim. Acta*, **45**, 33–51.
- HUTCHISON, R., ALEXANDER, C. M. O. and BARBER, D. J. (1987): The Semarkona meteorite; First recorded occurrence of smectite in an ordinary chondrite, and its implications. *Geochim. Cosmochim. Acta*, **51**, 1875–1882.
- IKEDA, Y., KIMURA, M., MORI, H. and TAKEDA, H. (1981): Chemical compositions of matrices of unequilibrated ordinary chondrites. *Mem. Natl. Inst. Polar Res., Spec. Issue*, **20**, 124–144.
- KOJIMA, H., YANAI, K. and IKADAI, S. (1985): Chromium distribution in type 3 ordinary chondrites. *Papers Presented to the Tenth Symposium on Antarctic Meteorites, 25–27 March 1985*. Tokyo, Natl. Inst. Polar Res., 43–44.
- KORNACKI, A. S. and WOOD, J. A. (1984): The mineral chemistry and origin of inclusion matrix and meteorite matrix in the Allende CV3 chondrite. *Geochim. Cosmochim. Acta*, **48**, 1663–1676.
- LARIMER, J. W. and ANDERS, E. (1967): Chemical fractionations in meteorites—II; Abundance patterns and their interpretation. *Geochim. Cosmochim. Acta*, **31**, 1239–1270.
- LARIMER, J. W. and ANDERS, E. (1970): Chemical fractionations in meteorites—III; Major element fractionations in chondrites. *Geochim. Cosmochim. Acta*, **34**, 367–387.
- LARIMER, J. W. and BARTHOLOMAY, M. (1979): The role of carbon and oxygen in cosmic gases; Some applications to the chemistry and mineralogy of enstatite chondrites. *Geochim. Cosmochim. Acta*, **43**, 1455–1466.
- MATSUNAMI, S. (1984): The chemical compositions and textures of matrices and chondrule rims of eight unequilibrated ordinary chondrites; A preliminary report. *Mem. Natl. Inst. Polar Res., Spec. Issue*, **35**, 126–148.
- MATSUNAMI, S. (1990): Kinetics of reaction between enstatite and metallic iron—I; Experimental

- results, possible reaction mechanism and the implications for the formation and accretion of chondritic materials in the early solar system. Submitted to *Geochim. Cosmochim. Acta*.
- MATSUNAMI, S., NISHIMURA, H. and TAKESHI, H. (1990): A simple model for non-equilibrium condensation of ferrous olivine in the early solar system. Submitted to *Earth Planet. Sci. Lett.*
- MYERS, J. and EUGSTER, H. P. (1983): The system Fe-Si-O; Oxygen buffer calibrations to 1,500K. *Contrib. Mineral. Petrol.*, **82**, 75–90.
- NAGAHARA, H. (1984): Matrices of type 3 ordinary chondrites—Primitive nebular records. *Geochim. Cosmochim. Acta*, **48**, 2581–2595.
- NAGAHARA, H. and KUSHIRO, I. (1987): Origin of iron-rich olivine in the matrices of type 3 ordinary chondrites; An experimental study. *Earth Planet. Sci. Lett.*, **85**, 537–547.
- OHMOTO, H. and KERRICK, D. (1977): Devolatilization equilibria in graphitic systems. *Am. J. Sci.*, **277**, 1013–1044.
- PALME, H. and FEGLEY, B., Jr. (1987): Formation of FeO-bearing olivines in carbonaceous chondrites by high temperature oxidation in the solar nebula. *Lunar and Planetary Science XVIII*. Houston, Lunar Planet. Inst., 754–755.
- RAMBALDI, E. R., FREDRIKSSON, B. J. and FREDRIKSSON, K. (1981): Primitive ultrafine matrix in ordinary chondrites. *Earth Planet. Sci. Lett.*, **56**, 107–126.
- RUBIN, A. E., FEGLEY, B. and BRETT, R. (1988): Oxidation state in chondrites. *Meteorites and the Early Solar System*, ed. by J. F. KERRIDGE and M. S. MATTHEWS. Tucson, Univ. Arizona Press, 488–511.
- SCOTT, E. R. D., RUBIN, A. E., TAYLOR, G. J. and KEIL, K. (1984): Matrix in type 3 chondrites—Occurrence, heterogeneity and relationship with chondrules. *Geochim. Cosmochim. Acta*, **48**, 1741–1757.
- SCOTT, E. R. D., BARBER, D. J., ALEXANDER, C. M. O., HUTCHISON, R. and PECK, J. A. (1988): Primitive material surviving in chondrites; Matrix. *Meteorites and the Early Solar System*, ed. by J. F. KERRIDGE and M. S. MATTHEWS. Tucson, Univ. Arizona Press, 718–745.
- SEARS, D. W. and WEEKS, K. S. (1983): Chemical and physical studies of type 3 chondrites; 2. Thermoluminescence of sixteen type 3 ordinary chondrites and relationships with oxygen isotopes. *Proc. Lunar Planet. Sci. Conf.*, 14th, Part 1, B301–B311 (*J. Geophys. Res.*, **88**, Suppl.).
- SEARS, D. W., GROSSMAN, J. N., MELCHER, C. L., ROSS, L. M. and MILLS, A. A. (1980): Measuring metamorphic history of unequilibrated ordinary chondrites. *Nature*, **287**, 791–795.
- SEARS, D. W., GROSSMAN, J. N. and MELCHER, C. L. (1982): Chemical and physical studies of type 3 chondrites—I; Metamorphism related studies of Antarctic and other type 3 ordinary chondrites. *Geochim. Cosmochim. Acta*, **46**, 2471–2481.
- WOOD, B. J. and KLEPPA, O. J. (1981): Thermochemistry of forsterite-fayalite olivine solutions. *Geochim. Cosmochim. Acta*, **45**, 529–534.
- WOOD, J. A. (1984): On the formation of meteoritic chondrules by aerodynamic drag heating in the solar nebula. *Earth Planet. Sci. Lett.*, **70**, 11–26.

(Received September 18, 1989; Revised manuscript received April 10, 1990)